The fiber type specificities of the different anti-rod domain antibodies in plectinopathy are presently unexplained.

It is also unclear why some patients with EBS-MD have myasthenic symptoms and others do not. Possibly myasthenic weakness of the limb muscles is masked by the MD, or is overlooked in severely weak patients, but fatigable weakness of the oculobulbar muscles would be unlikely to go unrecognized. It also is not known whether some mutations are more prone to result in the MyS phenotype than others.


## ACKNOWLEDGMENT

The authors thank Drs. Neill Graff-Radford and Nilufer Ertekin-Taner for anonymated DNA samples from African American control subjects.


## DISCLOSURE

Dr. Selcen reports no disclosures. Dr. Juel has received research support from Alexion Pharmaceuticals, Inc. Dr. Hobson-Webb has served as a consultant for Novella Clinical Inc. and has received research support from Genzyme Corporation and AANEM Foundation. Dr. Smith reports no disclosures. Dr. Stickler has received research support from Agency for Toxic Substances and Disease Registry, Centers for Disease Control and Prevention (CDC) and has served as an expert witness in a legal proceeding. Ms. Bite reports no disclosures. Dr. Ohno has received Grants-in-Aid from the Japan Society for the Promotion of Science, the Ministry of Health, Labour and Welfare, and the Japan Science and Technology Agency. Dr. Engel serves as an Associate Editor of *Neurology*; receives publishing royalties for *Myology 3rd ed.* (McGraw-Hill, 2004); and has received research support from the NIH and the Muscular Dystrophy Association.


*Received June 21, 2010. Accepted in final form September 21, 2010.*


## REFERENCES


1. Elliott CE, Becker B, Oehler S, Castanon MJ, Hauptmann R, Wiche G. Plectin transcript diversity: identification and tissue distribution of variants with distinct first coding exons and rodless isoforms. Genomics 1997;42:115–125.
2. Fuchs P, Zorer M, Rezniczek GA, et al. Unusual 5′ transcript complexity of plectin isoforms: novel tissue-specific exons modulate actin binding activity. Hum Mol Genet 1999;8:2461–2472.
3. Konieczny P, Fuchs P, Reipert S, et al. Myofiber integrity depends on desmin network targeting to Z-disks and costameres via distinct plectin isoforms. J Cell Biol 2008;181: 667–681.
4. Banwell BL, Russel J, Fukudome T, Shen X-M, Stilling G, Engel AG. Myopathy, myasthenic syndrome, and epidermolysis bullosa simplex due to plectin deficiency. J Neuropathol Exp Neurol 1999;58:832–846.
5. McLean W, Pulkkinen L, Smith F, et al. Loss of plectin causes epidermolysis bullosa with muscular dystrophy: cDNA cloning and genomic organization. Genes Dev 1996;10:1724–1735.
6. Smith FJ, Eady R, Leigh I, et al. Plectin deficiency results in muscular dystrophy and epidermolysis bullosa simplex. Nat Genet 1996;13:450–457.
7. Chavanas S, Pulkkinen L, Gache Y, et al. A homozygous nonsense mutation in the *PLEC1* gene in patients with epidermolysis bullosa simplex with muscular dystrophy. J Clin Invest 1996;98:2196–2200.
8. Pulkkinen L, Smith F, Shimizu H, et al. Homozygous deletion mutations in the plectin gene (PLEC1) in patients with epidermolysis bullosa simplex associated with late-onset muscular dystrophy. Hum Mol Genet 1996;5:1539–1546.
9. Gache Y, Chavanas S, Lacour J, et al. Defective expression of plectin/HD1 in epidermolysis bullosa simplex with muscular dystrophy. J Clin Invest 1996;97:2289–2298.
10. Mellerio J, Smith F, McMillan J, et al. Recessive epidermolysis bullosa simplex associated with plectin mutations: infantile respiratory complications in two unrelated cases. Br J Dermatol 1997;137:898–906.
11. Dang M, Pulkkinen L, Smith F, McLean W, Uitto J. Novel compound heterozygous mutations in the plectin gene in epidermolysis bullosa with muscular dystrophy and the use of protein truncation test for detection of premature termination codon mutations. Lab Invest 1998;78: 195–204.
12. Takizawa Y, Shimizu H, Rouan F, et al. Four novel plectin gene mutations in Japanese patients with epidermolysis bullosa and muscular dystrophy disclosed by heteroduplex scanning and protein truncation tests. J Invest Dermatol 1999;112:109–112.
13. Shimizu H, Takizawa Y, Pulkkinen L, et al. Epidermolysis bullosa simplex associated with muscular dystrophy: phenotype-genotype correlations and review of the literature. J Am Acad Dermatol 1999;41:950–956.
14. Rouan F, Pulkkinen L, Meneguzzi G, et al. Epidermolysis bullosa: novel and de novo premature termination codon and deletion mutations in the plectin gene predict late-onset muscular dystrophy. J Invest Dermatol 2000;114: 381–387.
15. Bauer JW, Rouan F, Kofler B, et al. A compound heterozygous one amino-acid insertion/nonsense mutation in the plectin gene causes epidermolysis bullosa simplex with plectin deficiency. Am J Pathol 2001;158:617–625.
16. Takahashi Y, Rouan F, Uitto J, et al. Plectin deficient epidermolysis bullosa simplex with 27-year-history of muscular dystrophy. J Dermatol Sci 2005;37:87–93.
17. Pfendner E, Rouan F, Uitto J. Progress in epidermolysis bullosa: the phenotypic spectrum of plectin mutations. Exp Dermatol 2005;14:241–249.
18. Bolling MC, Pas HH, De Visser M, et al. PLEC1 mutations underlie adult-onset dilated cardiomyopathy in epidermolysis bullosa simplex with muscular dystrophy. J Invest Dermatol 2010;130:1178–1181.
19. McMillan JR, Akiyama M, Rouan F, et al. Plectin defects in epidermolysis bullosa simplex with muscular dystrophy. Muscle Nerve 2007;35:24–35.
20. Rezniczeck GA, Walko G, Wiche G. Plectin defects lead to various forms of epidermolysis bullosa simplex. Dermatol Clin 2009;28:33–41.
21. Niemi K, Sommer H, Kero M, Kanerva L, Haltia M. Epidermolysis bullosa simplex associated with muscular dystrophy with recessive inheritance. Arch Dermatol 1988; 124:551–554.
22. Fine J-D, Stenn J, Johnson L, Wright T, Bock H, Horiguchi Y. Autosomal recessive epidermolysis bullosa simplex. Arch Dermatol 1989;125:931–938.
23. Doriguzzi C, Palmucci L, Mongini T, et al. Congenital muscular dystrophy associated with familial junctional epidermolysis bullosa letalis. Eur Neurol 1993;33:454–460.

24. Engel AG. The muscle biopsy. In: Engel AG, Franzini-Armstrong C, eds. Myology, 3rd ed. New York: McGraw-Hill; 2004:681–690.
25. Engel AG, Lambert EH, Howard FM. Immune complexes (IgG and C3) at the motor end-plate in myasthenia gravis: ultrastructural and light microscopic localization and electrophysiologic correlations. Mayo Clin Proc 1977;52:267–280.
26. Sahashi K, Engel AG, Lambert EH, Howard FM Jr. Ultrastructural localization of the terminal and lytic ninth complement component (C9) at the motor end-plate in myasthenia gravis. J Neuropathol Exp Neurol 1980;39:160–172.
27. Bodensteiner JB, Engel AG. Intracellular calcium accumulation in Duchenne dystrophy and other myopathies: a study of 567,000 muscle fibers in 114 biopsies. Neurology 1978;28:439–446.
28. Gautron J. Cytochimie ultrastructurale des acétylcholinestérases. Microscopie 1974;21:259–264.
29. Engel AG. Quantitative morphological studies of muscle. In: Engel AG, Franzini-Armstrong C, eds. Myology, 2nd ed. New York: McGraw-Hill; 1994:1018–1045.
30. Engel AG, Lindstrom JM, Lambert EH, Lennon VA. Ultrastructural localization of the acetylcholine receptor in myasthenia gravis and in its experimental autoimmune model. Neurology 1977;27:307–315.
31. Engel AG, Lambert EH, Mulder DM, et al. A newly recognized congenital myasthenic syndrome attributed to a prolonged open time of the acetylcholine-induced ion channel. Ann Neurol 1982;11:553–569.
32. Nastsuga K, Nishie W, Akiyama M, et al. Plectin expression patterns determine two distinct subtypes of epidermolysis bullosa simplex. Hum Mutat 2010;31:308–316.
33. Mokri B, Engel AG. Duchenne dystrophy: electron microscopic findings pointing to a basic or early abnormality in the plasma membrane of the muscle fiber. Neurology 1975;25:1111–1120.
34. Ruff RL. Effects of length changes on $Na^+$ current amplitude and excitability near and far from the end-plate. Muscle Nerve 1996;19:1084–1092.
35. Flucher BE, Daniels MP. Distribution of $Na^+$ channels and ankyrin in neuromuscular junctions is complementary to that of acetylcholine receptors and the 43 kd protein. Neuron 1989;3:163–175.
36. Ruff RL, Whittlesey D. $Na^+$ current density and voltage dependence in human intercostal muscle fibers. J Physiol 1992;458:85–97.
37. Ruff RL, Lennon VA. How myasthenia gravis alters the safety factor of neuromuscular transmission. J Neuroimmunol 2008;15:13–20.
38. Martin AR. Amplification of neuromuscular transmission by postjunctional folds. Proc R Soc Lond B 1994;258:321–326.
39. Konieczny P, Wiche G. Muscular integrity: a matter of interlinking distinct structures via plectin. In: Lang NG, ed. The Sarcomere and Skeletal Muscle Disease. New York: Springer; 2009:165–175.

Parkinsonism and Related Disorders 17 (2011) 46–49

Contents lists available at ScienceDirect

Parkinsonism and Related Disorders

journal homepage: www.elsevier.com/locate/parkreldis

# Urinary 8-hydroxydeoxyguanosine correlate with hallucinations rather than motor symptoms in Parkinson's disease☆

Masaaki Hirayama [a,*], Tomohiko Nakamura [a], Hirohisa Watanabe [a], Kei Uchida [a], Tetsuo Hama [a], Takashi Hara [a], Yoshiki Niimi [a], Mizuki Ito [a], Kinji Ohno [b], Gen Sobue [a,*]

[a] Department of Neurology, Nagoya University Graduate School of Medicine, 65 Tsurumai-cho, Showa-ku, Nagoya 466-8550, Japan
[b] Division of Neurogenetics, Center for Neurological Diseases and Cancer, Nagoya University Graduate School of Medicine, 65 Tsurumai-cho, Showa-ku, Nagoya 466-8550, Japan

ARTICLE INFO

*Article history:*
Received 11 August 2010
Received in revised form
27 October 2010
Accepted 1 November 2010

*Keywords:*
Parkinson's disease
8-Hydroxydeoxyguanosine
Hallucination
Oxidative stress
Non-motor symptom

ABSTRACT

*Background:* Oxidative stress is causally associated with the pathogenesis of Parkinson's disease (PD). Oxygen generates a large amount of reactive oxygen species (ROS). ROS including hydroxyl radicals and $H_2O_2$ react with guanine residues in DNA and produce 8-hydroxydeoxyguanosine (8-OHdG). 8-OHdG serves as a biomarker for oxidative stress in various diseases.
*Method:* We investigated urinary 8-OHdG levels in 61 PD patients and 28 normal subjects to evaluate the correlation with various clinical features. We quantified disease severity using the Unified Parkinson's Disease Rating Scale for motor symptoms (UPDRS part 3), the Mini-Mental State Examination (MMSE) for mental function, and the Tottori University Hallucination Rating Scale (TUHARS) for quantifying hallucinations.
*Results:* There were significant correlations between 8-OHdG and all the examined parameters, but the partial correlation coefficients excluding contributions of all the other parameters showed that only TUHARS and UPDRS part 3 are significantly related to 8-OHdG. In particular, TUHARS correlates best with urinary 8-OHdG levels.
*Conclusion:* The significant correlation between urinary 8-OHdG levels and hallucinations but not with dementia suggests that hallucinations are likely to have unique but unidentified mechanisms that lead to excessive production of 8-OHdG.



## 1. Introduction

Molecular oxygen is used by the body to produce energy, but it in turn generates a large amount of reactive oxygen species (ROS). These species cause oxidative stress in cells even in the presence of a diverse array of defense mechanisms against ROS. Oxidative stress is causally associated with aging and various diseases. ROS including hydroxyl radicals and $H_2O_2$ react with guanine residues in DNA and produce 8-hydroxydeoxyguanosine (8-OHdG). The oxidized guanosine is misread as an adenine in DNA replication, and is elaborately repaired to prevent accumulation of G-to-A mutations. The excised 8-OHdG is excreted in urine, thereby serving as a key biomarker of oxidative DNA damage. This oxidized guanine (8-OHdG) is also a marker for susceptibility to cancer [1,2], diabetes mellitus [3], and neurodegenerative diseases including Alzheimer's disease [4] and Parkinson disease (PD) [5,6]. Indeed, several lines of evidence implicate increased oxidative stress in the pathogenesis of PD. In PD, 8-OHdG levels are increased selectively in the substantia nigra [7] and also in serum and cerebrospinal fluid [8,9].

The clinical pathology of PD involves both motor and non-motor dysfunction. Non-motor symptoms are increasingly recognized as significant causes of morbidity in late stage PD. It is also recognized that some patients with PD present with prodromal non-motor symptoms in the absence of motor symptoms. We measured urinary 8-OHdG levels in PD patients and examined which clinical scores best dictate the 8-OHdG levels. To our surprise, we found that degrees of hallucination best correlated with the urinary 8-OHdG levels.

## 2. Methods

The study protocol was approved by the Human Ethics Review Committee of the Nagoya University Graduate School of Medicine, and all PD patients and normal subjects gave their written informed consent to the investigation.

☆ The review of this paper was entirely handled by an Associate Editor, Eng-King Tan.

* Corresponding authors.
*E-mail addresses:* hirasan@med.nagoya-u.ac.jp (M. Hirayama), sobueg@med.nagoya-u.ac.jp (G. Sobue).

1353-8020/$ – see front matter © 2010 Elsevier Ltd. All rights reserved.
doi:10.1016/j.parkreldis.2010.11.004

We recruited 70 patients with PD (mean age ± SD, 65.6 ± 8.4 years; range, 42–81) and 50 normal controls (56.6 ± 11.7 years; range, 31–87). Patients were recruited from consecutive outpatients seen in the Department of Neurology, Nagoya University Hospital, from September though December 2009. Patients with probable idiopathic PD were diagnosed according to published criteria [10]. Smokers, patients with diabetes mellitus, brain infarction, who had undergone deep brain stimulation and obese patients and obese controls were excluded from our study because they have high urinary 8-OHdG levels [11]. We analyzed 61 PD patients and 38 controls. Their clinical features are shown in Table 1. The onset represents the first recognition of motor impairment. We quantified disease severity using the Unified Parkinson's Disease Rating Scale for motor symptoms (UPDRS part 3), the Mini-Mental State Examination (MMSE) for mental function, and the Tottori University Hallucination Rating Scale (TUHARS) for quantifying hallucinations [12]. We employed TUHARS, because, in UPDRS, hallucinations are scored only in item 2 of part 1. The Parkinson Psychosis Questionnaire (PPQ) is able to quantify visual hallucinations [13], but PPQ is not appropriate for use with Japanese patients. The total TUHARS score correlates well with the hallucinations/illusions score in the PPQ ($r = 0.965$, $P < 0.001$) [12]. Although Scales for Outcomes of Parkinson's disease-COG, Parkinson's-cognitive rating scale, and Mini-mental Parkinson and Parkinson neuropsychometric dementia assessment scales are specifically designed to quantify cognitive impairment of PD [14], these scales have not been well validated in Japanese patients. We thus employed MMSE to estimate cognitive impairment.

Urine samples were obtained from each individual in the morning (9–12 AM) and immediately stored at −20 °C. We instructed the patients and controls to avoid physical activity in the 24 h before providing the sample. Urinary 8-OHdG concentrations were measured using an ELISA with a monoclonal antibody specific for 8-OHdG. Urinary 8-OHdG and creatinine (Cr) levels were anonymously measured by the Mitsubishi Chemical Medience Co. (Tokyo, Japan) [15]. Urinary 8-OHdG levels were normalized by urinary Cr levels to adjust for urine volumes.

As dopamine agonists reportedly induce hallucinations [16]. Dopamine agonists had already been discontinued in hallucinating PD patients before entry to this study, whereas non-hallucinating patients tended to be taking dopamine agonists. To avoid biases imposed by therapeutic interventions, we excluded dosage of dopamine agonists from our analysis.

Quantitative data are presented as means ± SD. We employed Student's *t*-test, Pearson's correlation coefficient, and multivariate analysis using the statistical package JMP8 (SAS Institute, Carry, NC). For the correlation analysis, *P* values less than 0.05 and correlation coefficients greater than 0.4 were considered to be significant. As clinical parameters are all related each other [5,6], we reanalyzed partial correlations to exclude contributions of all the other parameters.

## 3. Results

We observed a moderate correlation ($r = 0.35$, $P < 0.05$) between urinary 8-OHdG excretion and aging in normal individuals. Among the 38 controls, we thus selected 28 subjects (65.7 ± 7.7 years, 18 males at 64.0 ± 7.1 years, 10 females at 68.8 ± 9.1 years) of a minimum age of 55 years to match the ages of PD patients. Our cohort of 61 PD patients comprised 29 males (65.1 ± 8.6 years) and 32 females (65.1 ± 8.0 years) with a mean age of 65.1 ± 8.3 years. Urinary 8-OHdG levels ranged from 5.4 to 12.0 ng/mg Cr (mean 8.8 ± 1.6) in the 28 controls, and 4.8 to 23.8 ng/mg Cr (mean 10.7 ± 4.0) in the 61 PD patients ($P < 0.01$). Urinary 8-OHdG levels were not significantly different between males and females in both controls (males, 8.6 ± 1.8 ng/mg Cr; females, 8.1 ± 2.1) and PD patients (males, 10.2 ± 3.6; females, 11.3 ± 4.3).

**Table 1**
Clinical features of 61 PD patients.

| Clinical features | Mean ± SD | Range |
|---|---|---|
| Age at examination (years) | 65.1 ± 8.3 | 42–81 |
| Duration from onset (years) | 7.7 ± 6.1 | 1–23 |
| Age at onset (years) | 56.8 ± 8.7 | 39–73 |
| Yahr | 2.8 ± 1.1 | 1–5 |
| UPDRS part 1 | 3.3 ± 3.2 | 0–13 |
| UPDRS part 2 | 11.8 ± 10.0 | 0–49 |
| UPDRS part 3 | 22.9 ± 16.9 | 1–87 |
| TUHARS | 4.24 ± 6.1 | 0–24 |
| MMSE | 28.4 ± 2.8 | 18–30 |
| Levodopa dose (mg/day) | 309 ± 216 | 0–1200 |

We assumed that the normal urinary 8-OHdG levels were no more than 12 ng/mg Cr (mean + 2SD of 28 controls). We thus divided 61 PD patients into two groups with high (>12 ng/mg Cr, 17patients) and normal (≤12 ng/mg Cr, 44 patients) 8-OHdG levels. We found that the age at time of study, the disease duration, UPDRS part 3, TUHARS, MMSE and the levodopa dose were significantly higher in the high 8-OHdG group (Table 2). Similarly, we also found that the 8-OHdG levels demonstrate significant correlations with the age at examination, the disease duration, UPDRS part 3, TUHARS, MMSE, and the levodopa dose (Table 3). Among these, TUHARS showed the highest correlation coefficient. As the clinical parameters are mutually related each other, we calculated partial correlation coefficients ($r'$) to exclude contributions of other parameters and to delineate contribution of each parameter to the 8-OHdG levels. The partial correlation analysis revealed that the age at time of study, the disease duration, MMSE, and the levodopa dose were not significantly related to the 8-OHdG levels, while TUHARS and UPDRS part 3 were significantly related to 8-OHdG (Table 3). As the $r'$ value of TUHARS remained high after excluding effects of the other parameters, we plotted 8-OHdG against TUHARS and found that 40 out of 41 patients without hallucinations (98%) fell in the range of the mean ± 2SD of normal controls (5.6–12.0 ng/mg Cr) (Fig. 1).

## 4. Discussion

PD has been recognized as a movement disorder presenting with various motor symptoms, but there has been a gradual realization that PD is also associated with a broad spectrum of non-motor symptoms. These include anhedonia, depression, cognitive dysfunction, hallucinations, and complex behavioral disorders. Sato and colleagues previously reported that urinary 8-OHdG levels correlate to Hoehn and Yahr staging [5]. In this study, we quantified additional clinical features of PD, and found that urinary 8-OHdG levels correlate with all the examined clinical parameters except for age at onset. Among these, urinary 8-OHdG correlates most with hallucinations, yielding the correlation coefficient of 0.857 and the partial correlation coefficient of 0.761. Alam and colleagues reported increased 8-OHdG in the substantia nigra in PD [7]. Sato and colleagues postulated that high urinary 8-OHdG levels are possibly due to mitochondrial dysfunction in skeletal muscles because the substantia nigra is too small to generate a discernible amount of 8-OHdG [5]. Although our observations do not negate previous studies, urinary 8-OHdG is more likely to arise from dysfunction of neuronal cells and circuits that culminate in hallucinations. Hallucinations reportedly occur in 50% of patients with PD [17] and have a persistent and progressive nature [16]. Hallucinations experienced by PD patients have been postulated to occur via the following mechanisms: dopaminergic over-activity in the limbic system and cerebral cortices [18]; an imbalance with cholinergic neurotransmission [19]; dysfunction of the frontal areas associated with the control of attention [20]; PD-associated retinopathy [21]; decline of both image recognition speed and sustained attention

**Table 2**
Differences in clinical features between high and low urinary 8-OHdG levels in PD.

| Clinical parameter | High level $N = 17$ | Normal level $N = 44$ | *P* value |
|---|---|---|---|
| Age at onset | 56.5 ± 8.7 | 56.9 ± 8.8 | n.s. |
| Age at exam | 69.7 ± 7.5 | 63.3 ± 6.3 | $P < 0.01$ |
| Duration | 12.5 ± 7.5 | 5.9 ± 4.3 | $P < 0.001$ |
| UPDRS part 3 | 35.8 ± 19.1 | 17.7 ± 12.6 | $P < 0.0001$ |
| TUHARS | 12.6 ± 4.5 | 1.0 ± 2.3 | $P < 0.0001$ |
| MMSE | 26.5 ± 4.2 | 29.1 ± 1.6 | $P < 0.01$ |
| Levodopa dose | 441 ± 212 | 257 ± 197 | $P < 0.01$ |

**Table 3**
Correlation coefficients ($r$) and partial correlation coefficients ($r'$) normalized for all the other factors between 8-OHdG and the indicated clinical parameters.

| Clinical parameter | $r$ | $P$ value | $r'$ | $P$ value |
|---|---|---|---|---|
| Age at exam | 0.336 | <0.05 | 0.062 | n.s. |
| Duration | 0.594 | <0.0001 | 0.021 | n.s. |
| UPDRS part 3 | 0.615 | <0.0001 | 0.275 | <0.05 |
| TUHARS | 0.857 | <0.0001 | 0.761 | <0.0001 |
| MMSE | −0.499 | <0.0001 | −0.213 | n.s. |
| Levodopa dose | 0.522 | <0.0001 | 0.122 | n.s. |

n.s., not significant.

[22]; alterations of brainstem sleep-wake and dream regulation [23]. Hallucinations are also associated with myocardial sympathetic dysfunction in PD [24]. Dysregulation of β1-adrenergic system in PD tends to cause myocardial tachycardia [25], which may increase the myocardial oxidative stress. In addition hallucinating patients show significantly lower cerebral blood flow in temporal regions, the inferior parietal lobule, precuneus gyrus, and occipital cortex than non-hallucinating patients [26,27], which may increase cerebral oxidative stress. Motor dysfunctions are mostly due to degeneration of the substantia nigra and related structures, whereas hallucinations are likely to represent more extensive impairment of cerebral nuclei and cortices. The difference in the number of affected neurons may explain why increased urinary 8-OHdG levels correlated more with hallucinations than motor symptoms. Although PD patients with hallucinations frequently develop dementia and show widespread atrophy involving limbic, paralimbic, and neocortical areas [28], the partial correlation coefficient between 8-OHdG and MMSE was lower than TUHARS in our patients. This also suggests that the number of affected neurons alone does not simply account for the increased urinary 8-OHdG levels. Hallucinations should represent neuronal hyperactivity, whereas dementia is caused by loss of neuronal activities. The difference in the ways the neurons are affected may explain why 8-OHdG correlates with hallucinations but not with dementia.

The MMSE inevitably has floor effects in subjects with severe cognitive impairment and ceiling effects in subjects with mild cognitive impairment in PD [14], however, other cognitive impairment scales that are specifically designed for PD have not been well validated in Japanese patients with PD. Further studies are required to estimate the correlation between 8-OHdG and PD-specific cognitive impairments.

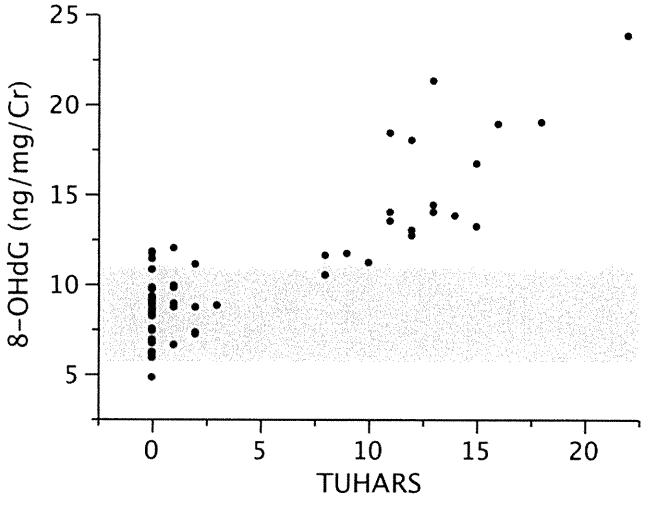


**Fig. 1.** Urinary 8-OHdG levels are plotted against TUHARS scores. Shaded area indicates the mean ± 2SD of 8-OHdG in age-matched controls.

In our studies, we only quantified degrees of hallucinations and cognitive impairments. PD is also associated with a broad spectrum of non-motor symptoms including sleepiness, depression, autonomic dysfunctions, and complex behavioral disorders. Quantification of other non-motor symptoms is required to conclude if other factors are also associated with elevated urinary 8-OHdG levels.

## Financial disclosure

None of the authors have any financial disclosures.

## Competing interests

None.

## Acknowledgements

This work was supported by Grants-in-Aid from the Ministry of Education, Culture, Sports, Science, and Technology of Japan, and the Ministry of Health, Labor, and Welfare of Japan.

## References

[1] Erhola M, Toyokuni S, Okada K, Tanaka T, Hiai H, Ochi H, et al. Biomarker evidence of DNA oxidation in lung cancer patients: association of urinary 8-hydroxy-2′-deoxyguanosine excretion with radiotherapy, chemotherapy, and response to treatment. FEBS Lett 1997;409:287–91.
[2] Halliwell B, Zhao K, Whiteman M. The gastrointestinal tract: a major site of antioxidant action? Free Radic Res 2000;33:819–30.
[3] Leinonen J, Lehtimaki T, Toyokuni S, Okada K, Tanaka T, Hiai H, et al. New biomarker evidence of oxidative DNA damage in patients with non-insulin-dependent diabetes mellitus. FEBS Lett 1997;417:150–2.
[4] Mecocci P, Polidori MC, Ingegni T, Cherubini A, Chionne F, Cecchetti R, et al. Oxidative damage to DNA in lymphocytes from AD patients. Neurology 1998;51:1014–7.
[5] Sato S, Mizuno Y, Hattori N. Urinary 8-hydroxydeoxyguanosine levels as a biomarker for progression of Parkinson disease. Neurology 2005;64:1081–3.
[6] Chen CM, Liu JL, Wu YR, Chen YC, Cheng HS, Cheng ML, et al. Increased oxidative damage in peripheral blood correlates with severity of Parkinson's disease. Neurobiol Dis 2009;33:429–35.
[7] Alam ZI, Jenner A, Daniel SE, Lees AJ, Cairns N, Marsden CD, et al. Oxidative DNA damage in the parkinsonian brain: an apparent selective increase in 8-hydroxyguanine levels in substantia nigra. J Neurochem 1997;69:1196–203.
[8] Kikuchi A, Takeda A, Onodera H, Kimpara T, Hisanaga K, Sato N, et al. Systemic increase of oxidative nucleic acid damage in Parkinson's disease and multiple system atrophy. Neurobiol Dis 2002;9:244–8.
[9] Gmitterova K, Heinemann U, Gawinecka J, Varges D, Ciesielczyk B, Valkovic P, et al. 8-OHdG in cerebrospinal fluid as a marker of oxidative stress in various neurodegenerative diseases. Neurodegener Dis 2009;6:263–9.
[10] Gelb DJ, Oliver E, Gilman S. Diagnostic criteria for Parkinson disease. Arch Neurol 1999;56:33–9.
[11] van Zeeland AA, de Groot AJ, Hall J, Donato F. 8-Hydroxydeoxyguanosine in DNA from leukocytes of healthy adults: relationship with cigarette smoking, environmental tobacco smoke, alcohol and coffee consumption. Mutat Res 1999;439:249–57.
[12] Wada-Isoe K, Ohta K, Imamura K, Kitayama M, Nomura T, Yasui K, et al. Assessment of hallucinations in Parkinson's disease using a novel scale. Acta Neurol Scand 2008;117:35–40.
[13] Dubois B, Burn D, Goetz C, Aarsland D, Brown RG, Broe GA, et al. Diagnostic procedures for Parkinson's disease dementia: recommendations from the movement disorder society task force. Mov Disord 2007;22:2314–24.
[14] Kulisevsky J, Pagonabarraga J. Cognitive impairment in Parkinson's disease: tools for diagnosis and assessment. Mov Disord 2009;24:1103–10.
[15] Omata N, Tsukahara H, Ito S, Ohshima Y, Yasutomi M, Yamada A, et al. Increased oxidative stress in childhood atopic dermatitis. Life Sci 2001;69:223–8.
[16] Goetz CG, Leurgans S, Pappert EJ, Raman R, Stemer AB. Prospective longitudinal assessment of hallucinations in Parkinson's disease. Neurology 2001;57:2078–82.
[17] Williams DR, Lees AJ. Visual hallucinations in the diagnosis of idiopathic Parkinson's disease: a retrospective autopsy study. Lancet Neurol 2005;4:605–10.
[18] Wolters EC, Francot CM. Mental dysfunction in Parkinson's disease. Parkinsonism Relat Disord 1998;4:107–12.
[19] Manganelli F, Vitale C, Santangelo G, Pisciotta C, Iodice R, Cozzolino A, et al. Functional involvement of central cholinergic circuits and visual hallucinations in Parkinson's disease. Brain 2009;132:2350–5.
[20] Ramirez-Ruiz B, Marti MJ, Tolosa E, Falcon C, Bargallo N, Valldeoriola F, et al. Brain response to complex visual stimuli in Parkinson's patients with

hallucinations: a functional magnetic resonance imaging study. Mov Disord 2008;23:2335–43.
[21] Devos D, Tir M, Maurage CA, Waucquier N, Defebvre L, Defoort-Dhellemmes S, et al. ERG and anatomical abnormalities suggesting retinopathy in dementia with Lewy bodies. Neurology 2005;65:1107–10.
[22] Meppelink AM, Koerts J, Borg M, Leenders KL, van Laar T. Visual object recognition and attention in Parkinson's disease patients with visual hallucinations. Mov Disord 2008;23:1906–12.
[23] Kulisevsky J, Roldan E. Hallucinations and sleep disturbances in Parkinson's disease. Neurology 2004;63:S28–30.
[24] Kitayama M, Wada-Isoe K, Irizawa Y, Nakashima K. Association of visual hallucinations with reduction of MIBG cardiac uptake in Parkinson's disease. J Neurol Sci 2008;264:22–6.
[25] Nakamura T, Hirayama M, Ito H, Takamori M, Hamada K, Takeuchi S, et al. Dobutamine stress test unmasks cardiac sympathetic denervation in Parkinson's disease. J Neurol Sci 2007;263:133–8.
[26] Okada K, Suyama N, Oguro H, Yamaguchi S, Kobayashi S. Medication-induced hallucination and cerebral blood flow in Parkinson's disease. J Neurol 1999; 246:365–8.
[27] Matsui H, Nishinaka K, Oda M, Hara N, Komatsu K, Kubori T, et al. Hypoperfusion of the visual pathway in parkinsonian patients with visual hallucinations. Mov Disord 2006;21:2140–4.
[28] Ibarretxe-Bilbao N, Ramirez-Ruiz B, Junque C, Marti MJ, Valldeoriola F, Bargallo N, et al. Differential progression of brain atrophy in Parkinson's disease with and without visual hallucinations. J Neurol Neurosurg Psychiatr 2010;81:650–7.

Nucleic Acids Research Advance Access published February 2, 2011

*Nucleic Acids Research, 2011, 1–9*
*doi:10.1093/nar/gkr026*

# AG-dependent 3′-splice sites are predisposed to aberrant splicing due to a mutation at the first nucleotide of an exon

**Yuan Fu, Akio Masuda, Mikako Ito, Jun Shinmi and Kinji Ohno***

Division of Neurogenetics, Center for Neurological Diseases and Cancer, Nagoya University Graduate School of Medicine, 65 Tsurumai, Showa-ku, Nagoya 466-8550, Japan

Received October 10, 2010; Revised December 23, 2010; Accepted January 12, 2011

## ABSTRACT

**In pre-mRNA splicing, a conserved AG/G at the 3′-splice site is recognized by U2AF$^{35}$. A disease-causing mutation abrogating the G nucleotide at the first position of an exon ($E^{+1}$) causes exon skipping in *GH1*, *FECH* and *EYA1*, but not in *LPL* or *HEXA*. Knockdown of U2AF$^{35}$ enhanced exon skipping in *GH1* and *FECH*. RNA-EMSA revealed that wild-type *FECH* requires U2AF$^{35}$ but wild-type *LPL* does not. A series of artificial mutations in the polypyrimidine tracts of *GH1*, *FECH*, *EYA1*, *LPL* and *HEXA* disclosed that a stretch of at least 10–15 pyrimidines is required to ensure normal splicing in the presence of a mutation at $E^{+1}$. Analysis of nine other disease-causing mutations at $E^{+1}$ detected five splicing mutations. Our studies suggest that a mutation at the AG-dependent 3′-splice site that requires U2AF$^{35}$ for spliceosome assembly causes exon skipping, whereas one at the AG-independent 3′-splice site that does not require U2AF$^{35}$ gives rise to normal splicing. The AG-dependence of the 3′-splice site that we analyzed in disease-causing mutations at $E^{+1}$ potentially helps identify yet unrecognized splicing mutations at $E^{+1}$.**

## INTRODUCTION

In higher eukaryotes, generation of functional mRNA is dependent on the removal of introns from pre-mRNA by splicing (1). The splicing process occurs in the spliceosome, the major components of which include five small nuclear RNAs and their associated proteins (U1, U2, U4, U5 and U6 snRNPs) in addition to a large number of non-snRNP proteins (2). In the first step of assembly of the spliceosome, U1 snRNP, SF1, U2AF$^{65}$ and U2AF$^{35}$ bind to the splicing *cis*-elements at the 5′ splice site (ss), the branch point sequence (BPS), the polypyrimidine tract (PPT) and the acceptor site, respectively, to form complex E (3).

Yeast has a well conserved BPS of UACUAAC (4), whereas we recently reported that human carries a highly degenerate BPS of yUnAy, where '*y*' and '*n*' represent pyrimidines and any nucleotides, respectively (5). Degeneracy of the human BPS supports a notion that the human BPS is likely to be recognized along with the downstream PPT where U2AF$^{65}$ binds and possibly with the invariant AG dinucleotide at the 3′ ss where U2AF$^{35}$ binds (6,7). U2AF$^{65}$ and U2AF$^{35}$ also make a heterodimer (8). In PPT, uridines are preferred over cytidines (9,10). In addition, PPT with 11 continuous uridines is highly competent and the position of such PPT is not critical (10). On the other hand, PPTs with only five or six uridines are required to be located close the 3′ AG for efficient splicing. In addition, phosphorylated DEK binds to and cooperates with U2AF$^{35}$ for proper recognition of the 3′ ss (11).

In the next step of the spliceosome assembly, the bound U2AF$^{65}$ and U2AF$^{35}$ facilitate substitution of SF1 for U2snRNP at the branch point to form complex A. Introns carrying a long stretch of PPT do not require U2AF$^{35}$ for this substitution, which is called 'AG-independent 3′ ss' (12–15). On the other hand, introns with a short or degenerate PPT require both U2AF$^{65}$ and U2AF$^{35}$ for this substitution, which is called 'AG-dependent 3′ ss'. Thereafter, the U4/U6.U5 tri-snRNP is integrated into the spliceosome to form complex B and the initial assembly of the spliceosome is completed.

The invariant AG dinucleotides are frequently reported targets of mutations causing human diseases, and the most frequent consequence is skipping of one or more exons (16). In addition, even mutations in highly degenerate BPS (5) and PPT (17) give rise to aberrant splicing

*To whom correspondence should be addressed. Tel: +81 52 744 2446; Fax: +81 52 744 2449; Email: ohnok@med.nagoya-u.ac.jp

causing genetic diseases (18). Disease-causing mutations also affect the first nucleotide of an exon ($E^{+1}$), but their effects on pre-mRNA splicing have been rarely scrutinized. As far as we know, only three such mutations in *FECH* (19), *GH1* (20) and *EYA1* (21) have been reported to cause aberrant splicing. Similarly, two such mutations in *LPL* (22) and *HEXA* (23) have been reported to have no effect on splicing. In this communication, we dissected molecular bases that differentiate splicing-disrupting and splicing-competent mutations, and found that AG-dependent ss is vulnerable to a mutation at $E^{+1}$, whereas AG-independent ss is tolerant.

## MATERIALS AND METHODS

### Minigene constructs and mutagenesis

Human genes of our interest were PCR-amplified from HEK293 cells using the KOD plus DNA polymerase (Toyobo). We introduced restriction enzyme-recognition sites at the 5′-end of the forward and reverse primers. We inserted the amplicon into the pcDNA3.1(+) mammalian expression vector (Invitrogen). We introduced patients' or artificial mutations with the QuikChange site-directed mutagenesis kit (Stratagene). We confirmed the absence of unexpected artifacts with the CEQ8000 genetic analyzer (Beckman Coulter).

### Cell culture and transfection procedures

HEK293 cells were maintained in the Dulbecco's minimum essential medium (DMEM, Sigma-Aldrich) with 10% fetal bovine serum (FBS, Sigma-Aldrich). At ~50% confluency (~$5 \times 10^5$ cells) in a 12-well plate, 1 ml of fresh Opti-MEM I (Invitrogen) was substituted for DMEM, and 500 ng of a minigene with 1.5 µl of the FuGENE6 transfection reagent (Roche Diagnostics) were then added. After 4 h, 2 ml of DMEM with 10% FBS was overlaid, and the cells were incubated overnight. The transfection medium was replaced with 2 ml of fresh DMEM with 10% FBS. RNA was extracted at 48 h after initiation of transfection.

### RNA extraction and RT–PCR

Total RNA from HEK293 was extracted by Trizol reagent (Invitrogen) according to the manufacturer's protocols. The quantity and quality of RNA was determined by spectrophotometry (NanoDrop Techonologies). Twenty percent of the isolated RNA was used as a template for cDNA synthesis with the Oligo(dT) 12–18 Primer (Invitrogen) and the ReverTra Ace (Toyobo). Ten percent of the synthesized cDNA was used as a template for RT–PCR amplification with T7 primer (5′-TAATACG ACTCACTATAGGG-3′) and gene-specific primers for minigenes in pcDNA3.1(+). Image J software (National Institutes of Health) was used to quantify intensities of fragments. We employed JMP (SAS Institute) for statistical analysis.

### RNA interference to knockdown U2AF$^{35}$

We synthesized siRNA of 5′-GGCUGUGAUUGACUU GAAUdTdT-3′ (GenBank accession number NM_006758, nucleotides 459–479), which is against the shared sequence of U2AF$^{35}$a and U2AF$^{35}$b (15). We employed Lipofectamine 2000 (Invitrogen) to cotransfect plasmids and siRNAs according to the manufacturer's protocols. Briefly, the transfection reagent included 300 ng of the plasmid, 50 pmol of siRNA, and 2 µl of lipofectamine 2000 in 100 µl of Opti-MEM I. The cells were harvested by western blotting for 48 h after transfection. The primary antibodies were goat polyclonal antibody for U2AF$^{35}$ (Santa Cruz Biotechnology), and mouse monoclonal antibodies for U2AF$^{65}$ (Santa Cruz Biotechnology) and PTB (Zymed Laboratories). The secondary antibodies were HRP-conjugated mouse anti-goat (Santa Cruz Biotechnology) or sheep anti-mouse (GE healthcare) antibodies. The immunoreactive proteins were detected by enhanced chemiluminescence (ECL, Amersham Biosciences).

For the siRNA rescue assay, we cloned the human U2AF$^{35}$ cDNA (Open Biosystems) into the HindIII and EcoRI restriction sites of the p3XFLAG-CMV-14 vector (Sigma-Aldrich). We introduced four silent mutations into the siRNA target region using the QuikChange site-directed mutagenesis kit with a primer, 5′-GAAAAG GCTGTAATCGATTTAAATAACCGTTGGTT-3′, where artificial mutations are underlined (24).

### RNA probe synthesis

We synthesized [α-$^{32}$P]-CTP-labeled RNA using the Riboprobe *in vitro* transcription system (Promega) from a PCR-amplified fragment according to the manufacturer's instructions. We used the same forward primer for all the probes with the sequence of 5′-*TAATACGACTCACT ATAGG*GAGACAGG-3′, where the italicized is T7 promoter and the underlined is for annealing to the reverse primer. The four reverse primers were: wild-type *FECH*, 5′-TGGACCAACCTATGCGAAAGATAGACG AATGCGTAAGCCTGTCTC-3′; mutant *FECH*, 5′-TGG ACCAAACTATGCGAAAGATAGACGAATGCGTA AGCCTGTCTC-3′; wild-type *LPL*, 5′-TGGATCGAGG CCTTAAAAGGGAAAAAAGCAGGAACACCCTGT CTC-3′; and mutant *LPL*, 5′-TGGATCGAGGACTTAA AAGGGAAAAAAGCAGGAACACCCTGTCTC-3′, where the underlined is for annealing to the forward primer.

### Expression and purification of recombinant proteins

The human U2AF$^{35}$ and U2AF$^{65}$ cDNAs were obtained from Open Biosystems. U2AF$^{35}$ and U2AF$^{65}$ cDNAs were subcloned into the *Bam*HI and *Eco*RI restriction sites of the pFastBac HTb vector. The recombinant baculoviruses were expressed using the Bac-to-Bac Baculovirus Expression System (Invitrogen) according to the manufacturer's instructions. Infected Sf9 cells were harvested after 48 h and resuspended in the lysis buffer containing 50 mM sodium phosphate, 10 mM imidazole, 300 mM NaCl, 1% Triton X-100, 2 mM

β-mercaptoethanol, the Complete Protease Inhibitor Cocktail (Roche Applied Science) and 5 U endonuclease in pH 7.0. His-tagged $U2AF^{35}$ and $U2AF^{65}$ proteins were purified using the TALON metal affinity resins (Clontech) under the denatured and native conditions, respectively. Purified $U2AF^{35}$ was refolded by extended dialysis in dialysis buffer (50 mM sodium phosphate, 300 mM NaCl, 150 mM imidazole, pH 7.0). We determined the protein concentrations using the Pierce 660 nm Protein Assay Reagent (Thermo Scientific).

### RNA-electrophoretic mobility shift assay

The radioactively labeled RNA ($1 \times 10^5$ cpm) was incubated at room temperature with varying concentrations of recombinant proteins, 16 μg of yeast tRNA, and 1.6 U of RNasin (Toyobo) in a final volume of 20 μl of the binding buffer (20 mM HEPES pH 7.8, 50 mM KCl, 3 mM $MgCl_2$, 0.5 mM dithiothreitol, 0.5 mM EDTA and 5% glycerol). After 20 min, the RNA–protein complexes were separated on 5% non-denaturing polyacrylamide gels in 1 × TBE buffer at 4°C. The gels were dried and complex formation was visualized using the Typhoon 8600 Imager (GE Healthcare).

### *In silico* analysis of the human genome and ESE-motifs

We analyzed human genome annotations (NCBI Build 37.1, hg19) by writing Perl programs, and executing them either on the PrimePower HPC2500/Solaris 9 supercomputer (Fujitsu) or on the cygwin UNIX emulator running on a Windows computer. To search for ESE-motifs, we used the ESE Finder (http://rulai.cshl.org/ESE/) (25,26), the RESUCE-ESE server (http://genes.mit.edu/burgelab/rescue-ese/) (27), the FAS-ESS server (http://genes.mit.edu/fas-ess/) (28), the PESX server (http://cubweb.biology.columbia.edu/pesx/) (29,30), and the ESRsearch server (http://ast.bioinfo.tau.ac.il/) (31).

## RESULTS

### Recapitulation of normal and aberrant splicing in minigenes

We first constructed minigenes of *GH1*, *FECH*, *EYA1*, *LPL* and *HEXA*, and introduced a previously reported disease-causing mutation at $E^{+1}$ (Figure 1A). These minigenes successfully recapitulated normal and aberrant splicings: mutations in *GH1*, *FECH* and *EYA1* caused exon skipping, whereas those in *LPL* or *HEXA* did not (Figure 1B).

### Down-regulation of $U2AF^{35}$ increased exon skipping in wild-type *GH1* and *FECH*, but not in wild-type *EYA1*, *LPL* and *HEXA*

We predicted that a mutation at $E^{+1}$ should disrupt binding of $U2AF^{35}$. We thus hypothesized that *GH1*, *FECH* and *EYA1* require binding of $U2AF^{35}$ for the assembly of spliceosome, whereas *LPL* and *HEXA* do not require it. To prove this hypothesis, we first knocked down $U2AF^{35}$ and analyzed its effect on the wild-type minigenes. We achieved an efficient down-regulation of $U2AF^{35}$ in HEK293 cells (Figure 2A). We also confirmed

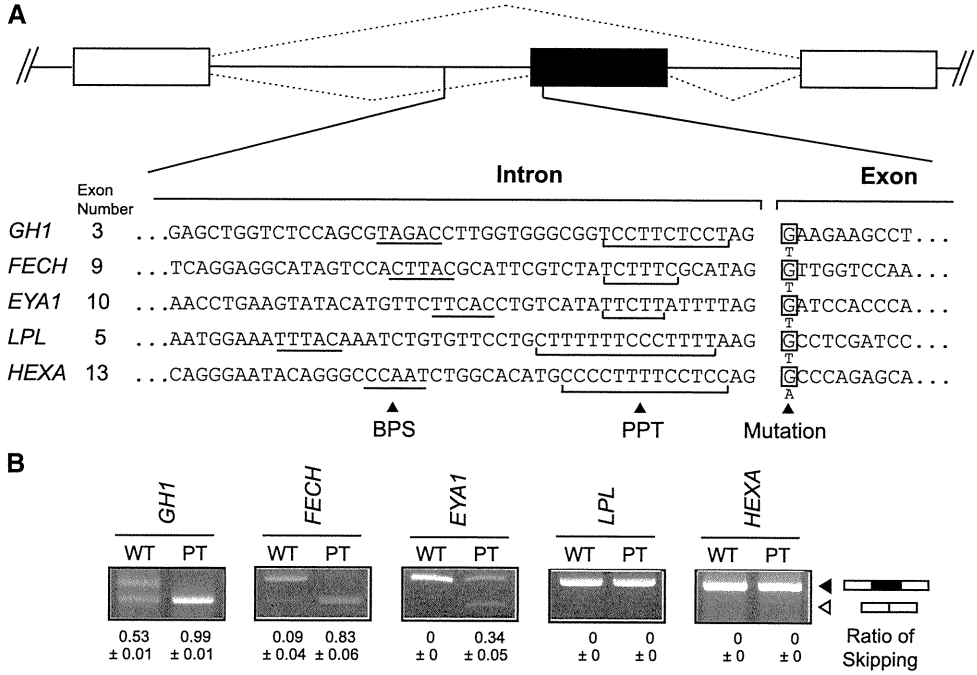


**Figure 1.** Recapitulation of normal and aberrant splicing of five genes. (**A**) Nucleotide sequences at the intron/exon junctions of five analyzed genes. Putative BPS is underlined. PPT is shown by a bracket. Mutant nucleotides are indicated at $E^{+1}$. (**B**) RT–PCR of minigenes expressed in HEK293 cells carrying the wild-type (WT) or patient's (PT) nucleotide. The mutations cause exon skipping in *GH1*, *FECH* and *EYA1*, but not in *LPL* and *HEXA*. Mean and SD of three independent experiments of the densitometric ratios of the exon-skipped product is shown at the bottom.

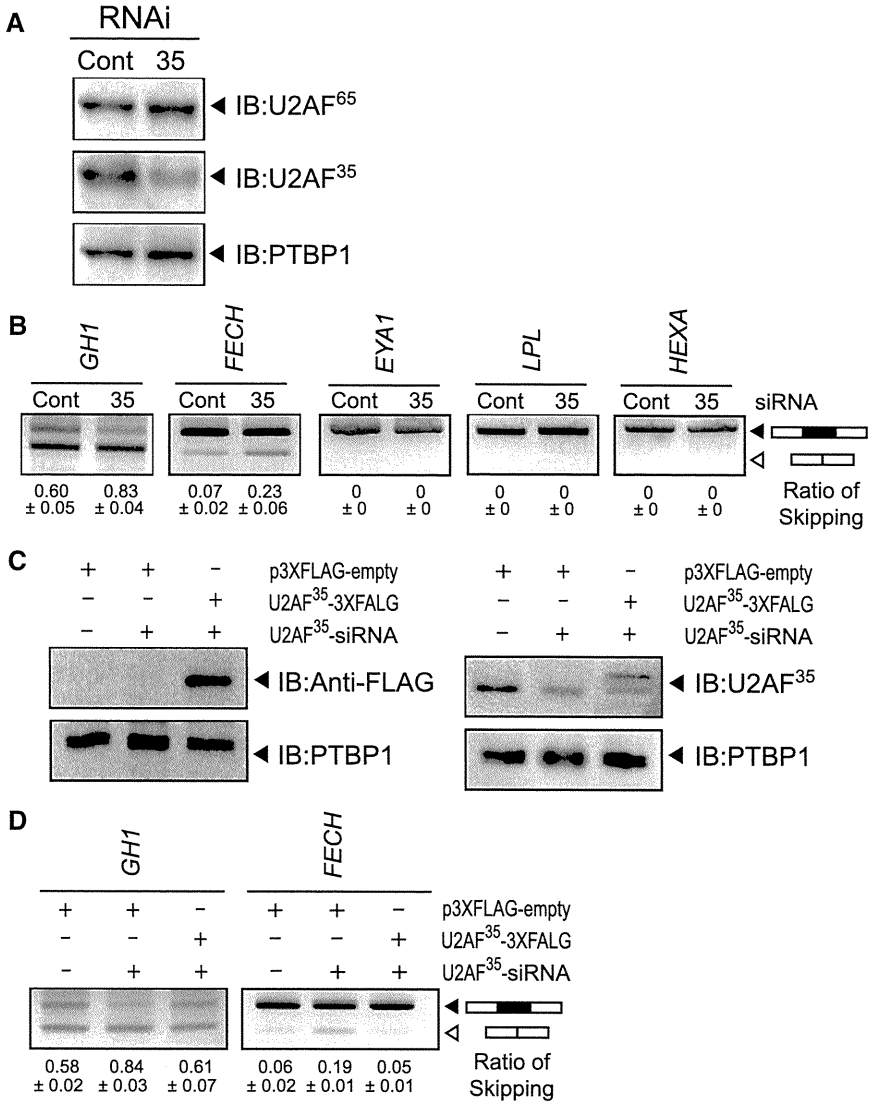


**Figure 2.** Effects of down-regulation of U2AF$^{35}$ on pre-mRNA splicing. (**A**) Western blots demonstrating that U2AF$^{35}$-siRNA efficiently knocks down U2AF$^{35}$ but not U2AF$^{65}$ or PTBP1. (**B**) Down-regulation of U2AF$^{35}$ facilitates exon skipping in wild-type *GH1* and *FECH*, but not in wild-type *EYA1*, *LPL* and *HEXA*. (**C**) Introduction of an siRNA-resistant p3XFLAG-U2AF$^{35}$ encoding 3× FLAG fused with U2AF$^{35}$ is visualized by immunoblots against FLAG and U2AF$^{35}$. (**D**) Exon skipping facilitated by U2AF$^{35}$-siRNA is partially rescued by introduction of the siRNA-resistant p3XFLAG-U2AF$^{35}$.

that the U2AF$^{35}$-siRNA had no effect on the expression level of U2AF$^{65}$. As expected, the down-regulation of U2AF$^{35}$ increased exon skipping of *GH1* and *FECH* (Figure 2B) but not to the levels of the mutant constructs (Figure 1B). Again, as expected, we observed no effect on *LPL* and *HEXA*. Unexpectedly, however, *EYA1* demonstrated no response to the down-regulation of U2AF$^{35}$. Less efficient effects of U2AF$^{35}$-siRNA on *GH1*, *FECH* and *EYA1* (Figure 2B) compared to the mutant constructs (Figure 1B) were likely because the mutation abolished binding of U2AF$^{35}$ in all the cells, whereas substantial numbers of cells failed to incorporate U2AF$^{35}$-siRNA and gave rise to normally spliced products.

We additionally introduced the siRNA-resistant p3XFLAG-U2AF$^{35}$ to ensure that the effect of siRNA-U2AF$^{35}$ was not due to off-target effects (Figure 2C). As expected, coexpression of p3XFLAG-U2AF$^{35}$ partially rescued the splicing defects in *GH1* and *FECH* (Figure 2D).

### U2AF$^{35}$ is required for binding of U2AF$^{65}$ to PPT in *FECH* but not in *LPL*

To further prove that U2AF$^{35}$ is required for pre-mRNA splicing, we employed an electrophoretic mobility shift assay (EMSA) using wild-type and mutant RNA substrates of *FECH* and *LPL* (Figure 3A). His-tagged U2AF$^{35}$ and U2AF$^{65}$ were expressed using bacluovirus and were purified under denatured and native conditions, respectively. Denatured U2AF$^{35}$ was refolded before RNA-EMSA. As expected, U2AF$^{65}$ failed to bind to the wild-type *FECH* in the absence of U2AF$^{35}$, and addition

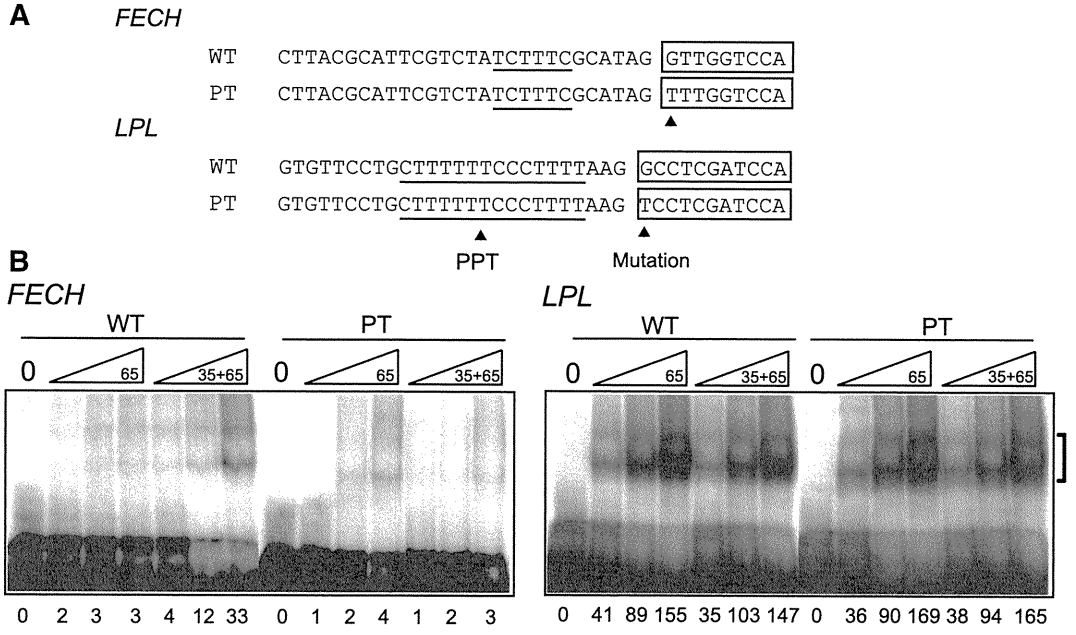


**Figure 3.** RNA-EMSA. (**A**) Sequences of wild-type (WT) and mutant (PT) RNA probes of *FECH* and *LPL* employed for RNA-EMSA. (**B**) RNA-EMSA of wild-type and mutant *FECH* and *LPL* with increasing amounts of $U2AF^{65}$ with or without $U2AF^{35}$. His-tagged $U2AF^{65}$ and $U2AF^{35}$ are expressed in Sf9 cells and are purified. Wild-type *FECH* requires $U2AF^{35}$ to bind to $U2AF^{65}$, whereas wild-type *LPL* does not require $U2AF^{35}$. A mutation at $E^{+1}$ abrogates binding of $U2AF^{65}$ in *FECH* but not in *LPL*. Concentrations of $U2AF^{35}$ are 5, 10 and 20 ng/μl; and those of $U2AF^{65}$ are 10, 20 and 40 ng/μl. Numbers at the bottom indicate intensities of the retarded fragments in arbitrary units.

of $U2AF^{35}$ gained its binding. For the mutant *FECH*, neither $U2AF^{65}$ alone nor addition of both U2AFs showed binding of U2AFs. On the other hand, the wild-type *LPL* did not require $U2AF^{35}$ to bind to $U2AF^{65}$. Addition of $U2AF^{35}$ did not substantially increased binding of $U2AF^{65}$. These bindings were not affected by the mutation at $E^{+1}$ of *LPL* (Figure 3B).

These results indicate that the mutation in *FECH* compromises a binding affinity for $U2AF^{35}$, which in turn abrogates binding of $U2AF^{65}$ and results in aberrant splicing. On the other hand, wild-type *LPL* does not need to bind to $U2AF^{35}$ and the mutation at $E^{+1}$ has no effect on the assembly of spliceosome.

### PPT determines the splicing consequences of the mutations

In an effort to delineate effects of the PPT sequences on the splicing consequence of a mutation at $E^{+1}$, we introduced a series of mutations into the PPT in the presence of the mutation at $E^{+1}$. Extensions of the polypyrimidine stretch ameliorated aberrant splicing in *GH1*, *FECH* and *EYA1*. Conversely, truncations or disruptions of the polypyrimidine stretch caused exon skipping in *LPL* and *HEXA* (Figure 4).

### Length of the polypyrimidine stretch best predicts the splicing consequences

We next sought for parameters that differentiate normal and aberrant splicings in these minigenes. Analysis of parameters that potentially dictate the strength of the PPT indicated that the length of pyrimidine stretch, the number of pyrimidines in 25 or 50 nt at the 3′-end of an intron correlated with the ratio of exon skipping with correlation coefficients of more than 0.6 (Supplementary Table S1). The number of pyrimidines in 25 or 50 nt at the 3′-end of an intron, however, failed to predict splicing consequences of nine other constructs shown in Figure 6, and is likely to be overfitted parameters unique to the 35 constructs in Figure 4. Coolidge and colleagues report that $(GU)_{11}$ in PPT is partly functional, but we did not observe alternative purine and pyrimidine residues in our PPTs and did not quantify effects of alternative nucleotides (10). We thus took the length of pyrimidine stretch as a best parameter to dictate the strength of the PPT (Figure 5A). The native *GH1*, *FECH* and *EYA1* carry a stretch of 6–10 pyrimidines, whereas the native *LPL* and *HEXA* harbor a stretch of 14 and 13 pyrimidines, respectively (arrows in Figure 5A). For highly degenerate PPTs in the artificial constructs, the total number of pyrimidines in a stretch of 25 nt at the 3′-end of an intron well predicts the ratio of exon skipping (Figure 5B). These analyses revealed that the length of the polypyrimidine stretch should be at least 10–15 nt to ensure normal splicing even in the presence of a mutation at $E^{+1}$.

### Identification of effects on pre-mRNA splicing of nine disease-associated mutations at the first nucleotide of an exon

We next examined other mutations at $E^{+1}$ in which splicing consequences have not been previously analyzed. We first identified 224 mutations that abrogate the first 'G' nucleotide of an exon in the Human Gene Mutation Database at http://www.hgmd.cf.ac.uk/ (data not shown). Among these, we arbitrarily chose nine mutations causing

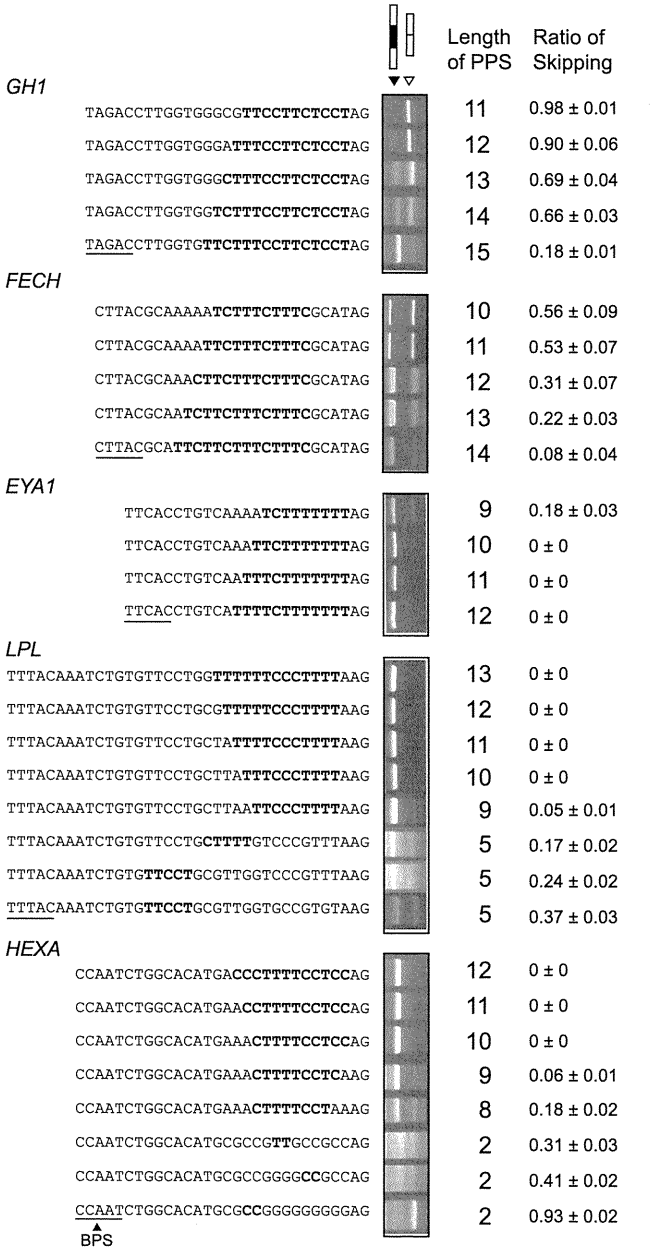


**Figure 4.** RT–PCR of HEK293 cells transfected with minigenes carrying artificially extended or disrupted PPT's. All the constructs harbor a mutation at $E^{+1}$. The top construct of each gene represents the patient's sequence. Only the nucleotide sequences of the 3′-end of an intron are indicated. The longest stretches of the polypyrimidines are shown in bold. Underlines indicate putative BPS's. The rightmost column shows the mean and SD of three independent experiments of the densitometric ratios of the exon-skipped product.

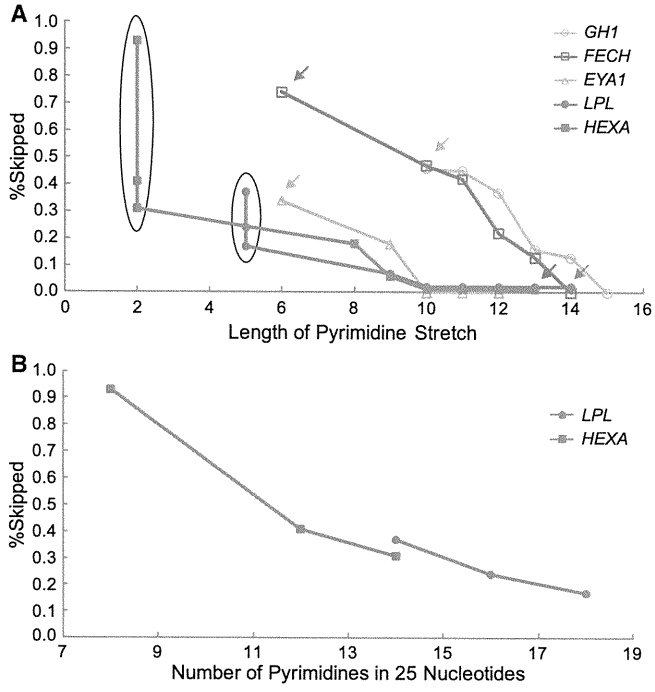


**Figure 5.** Ratios of exon skipping are plotted against the lengths of the polypyrimidine stretch (**A**) and the numbers of pyrimidines in 25 nt at the 3′-end of an intron (**B**). The ordinate (percent skipped) represents the ratios of exon skipping compared to that of the wild-type construct. The data are obtained from RT–PCR shown in Figure 4. Arrows indicate the original constructs carrying the patient's sequence, and the others are artificial constructs. Six constructs indicated by ovals in (A) are plotted in (B).

neuromuscular and musculoskeletal disorders (Figure 6A).

We constructed nine pairs of wild-type and mutant minigenes, and introduced them into HEK293 cells. We observed aberrant splicing in *PKHD1*, *COL1A2* (exon 37), *CLCN2*, *CAPN3* (exons 10 and 17), but not in *LAMA2*, *NEU1*, *COL6A2* and *COL1A2* (exon 23) (Figure 6B). The lengths of the polypyrimidine stretch of the five aberrantly spliced constructs ranged from 4 to 10 nt, whereas those of the four normally spliced constructs ranged from 9 to 16 nt. These results are in concordance with a notion that the short polypyrimidine stretches are predisposed to aberrant splicing due to a mutation at $E^{+1}$, whereas long polypyrimidine stretches are tolerant to such mutations. Among the 224 mutations affecting 'G' at $E^{+1}$, only three mutations have been reported to cause aberrant splicing. We here analyzed nine mutations and identified five more such mutations. It is thus likely that most splicing mutations at $E^{+1}$ still remain unrecognized to date.

## Analysis of the 3′-splice sites of the human genome

We next analyzed PPTs of 176 809 introns of the entire human genome. The length of the pyrimidine stretch was shorter when $E^{+1}$ was the conserved 'G' (Figure 7A). This also supports a notion that AG-dependent 3′ ss harboring G at $E^{+1}$ has a short polypyrimidine stretch (12). In addition, the ratio of 'C' at intronic position −3 was lower when $E^{+1}$ was the conserved 'G' (Figure 7B), which suggests that G at $E^{+1}$ makes C at −3 dispensable for binding to $U2AF^{35}$, although this is not directly relevant to the length of the PPT.

Being prompted by a previous report that $U2AF^{35}$ binds up to the 10th nucleotide of an exon (12), we examined nucleotide frequencies at exonic positions +1

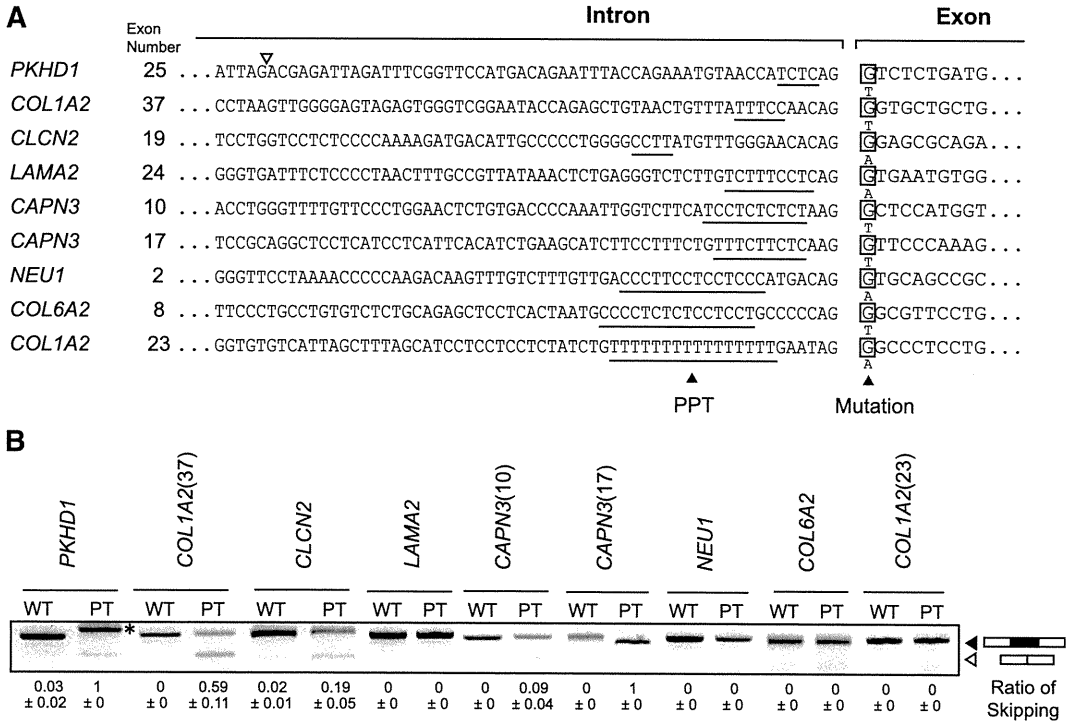


**Figure 6.** RT–PCR analysis of nine disease-causing mutations at $E^{+1}$. (**A**) Sequences at the intron/exon junctions of nine pairs of wild-type and mutant constructs. The longest polypyrimidine stretches are underlined. (**B**) RT–PCR of minigenes transfected into HEK293 cells. Five mutant constructs are aberrantly spliced, whereas the remaining four mutants are normally spliced. Numbers in the parentheses indicate exon numbers. In *PKHD1*, a cryptic 3′-splice site (open arrowhead in panel A) at 55 nt upstream of the native site is activated (asterisk). Mean and SD of three independent experiments of the densitometric ratios of the exon-skipped product is shown at the bottom.

to +12. We counted only wobbling nucleotides based on the human genome annotation NCBI Build 37.1 (hg19). As expected, 'GT' dinucleotide was frequently observed at exonic positions +1 and +2. We also observed preference for a 'T' nucleotide at positions +3 to +5 (Figure 7C). Alignment of SELEX results of $U2AF^{35}$ by Wu and colleagues (12) similarly demonstrate overrepresentation of 'T' nucleotides at positions +3 to +6 (Figure 7D). We thus analyzed effects of 'TTT' at positions +3 to +5 using the *GH1, FECH* and *EYA1* minigenes carrying the patient's mutations. We found that introduction of 'TTT' at exonic position +3 to +5 had no effect in *GH1* and *FECH*, but slightly enhanced exon recognition in *EYA1* (Figure 7E).

## DISCUSSION

We previously reported that the SD-score algorithm efficiently predicts splicing consequences of a mutation affecting the 5′ ss (32). We next identified that the human BPS consensus is simply yUnAy (5), and hoped to predict if a given mutation affecting the BPS causes aberrant splicing or not. The high degeneracy of the BPS consensus, however, prevented us from constructing an efficient algorithm. In this communication, we worked on mutations at $E^{+1}$. As far as we know, only three such mutations have been reported to cause aberrant splicing, and only two such mutations have been reported not to affect splicing. Knockdown and RNA-EMSA of $U2AF^{35}$, as well as analyses of artificial PPT mutations and nine disease-causing mutations at $E^{+1}$ revealed that AG-dependence of 3′ ss determines the splicing consequences. In the presence of a mutation at $E^{+1}$, a stretch of 15 or more pyrimidines ensures normal splicing, whereas a stretch of 10 or less pyrimidines are predisposed to aberrant splicing.

AG-dependent 3′ ss requires both $U2AF^{65}$ and $U2AF^{35}$ to bring U2snRNP to the branch point, whereas AG-independent 3′ ss has a long stretch of pyrimidines that can bind to $U2AF^{65}$ without $U2AF^{35}$ (13,15). $U2AF^{35}$ potentially provides an additional RNA–protein interacting force and an additional SR protein-binding surfaces (33). An artificial G-to-C mutation at $E^{+1}$ downstream of a stretch of five pyrimidines in the mouse IgM gene abrogates binding of $U2AF^{35}$ and causes defective splicing (14). Similarly, in *INSR* exon 11 carrying an 'A' nucleotide at $E^{+1}$, a stretch of 14 pyrimidines but not of 10 pyrimidines is properly spliced (34). Additionally, a stretch of eight pyrimidines upstream of the last exon with 'C' at $E^{+1}$ of *EIF3S7* is dependent on $U2AF^{35}$, whereas a stretch of 14 pyrimidines upstream of the last exon with 'A' at $E^{+1}$ of *CUEDC1* is independent (15). Our observations and previous reports all point to a notion that effects on pre-mRNA splicing should be scrutinized for a mutation at $E^{+1}$ if the preceding intron carries a short stretch of 10 or less pyrimidines. Indeed, in our analysis of nine disease-causing mutations, five of six mutants with 10 or less contiguous pyrimidines were aberrantly spliced (Figure 6), but no splicing analysis has been documented for any of them.

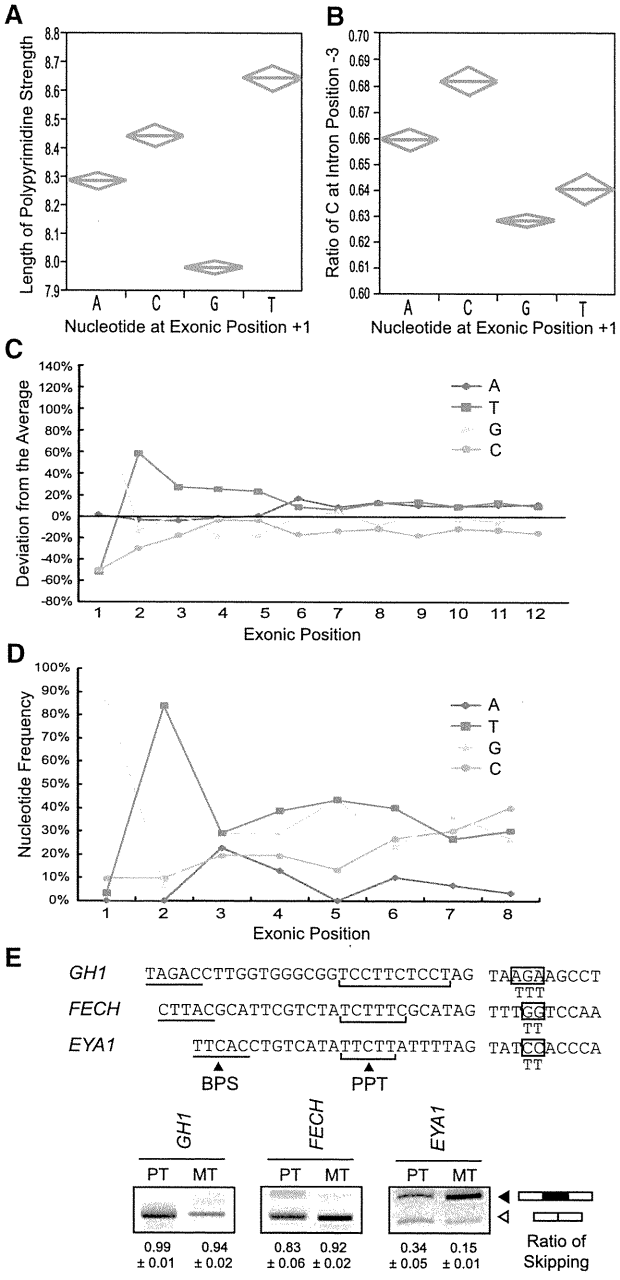


**Figure 7.** (**A**) Polypyrimidine stretch and the first nucleotide of an exon in the human genome. The longest stretch of uninterrupted pyrimidines among 25 nt at the 3′-ends of an intron is counted for 176 809 introns of the human genome. Diamonds represent means and 95% confidence intervals. One-way ANOVA and Fisher's-multiple range test revealed statistical significance of $P < 0.0001$. (**B**) Ratios of 'C' at position −3 in relation to the first nucleotide of an exon are analyzed for 176 809 introns of the human genome. Diamonds represent means and 95% confidence intervals. One-way ANOVA and Fisher's-multiple range test revealed statistical significance of $P < 0.0001$. (**C**) Preferentially observed nucleotides at the 5′-end of an exon in human. Only wobbling nucleotides are counted in the human genome. (**D**) Nucleotide frequencies at exonic positions +1 to +8 according to the SELEX data of U2AF$^{35}$ by Wu and colleagues (12). (**E**) Effects of 'TTT' at exonic positions +3 to +5 in *GH1*, *FECH* and *EYA1* carrying the patient's mutation at $E^{+1}$. Artificially substituted exonic nucleotides are indicated by boxes. Mean and SD of three independent experiments of the densitometric ratios of the exon-skipped product is shown at the bottom.

We first report overrepresentation of 'T' nucleotides at exonic positions +3 to +5 in the human genome, as well as in *in vitro* U2AF$^{35}$-binding sites. Enhancement of exon recognition in *EYA1* by introduction of 'TTT' at positions +3 to +5 also underscores a notion that 'TTT' at +3 to +5 is likely to enhance binding of U2AF$^{35}$. Effects of 'TTT', however, were not observed in *GH1* and *FECH*. As the patient's mutation in *GH1* and *FECH* resulted in almost complete skipping of an exon, whereas that in *EYA1* gave rise to both exon-skipped and included products. The degrees of aberration of exon recognition may account for the 'TTT'-responsiveness. Alternatively, although no ESE motif was detected in the 'TTT'-introduced *EYA1* by five different ESE search tools, an unrecognized ESE might have ameliorated exon skipping in *EYA1*. Further analysis is required to elucidate effects of overrepresentation of 'T' at positions +3 to +5.

## SUPPLEMENTARY DATA

Supplementary Data are available at NAR Online.

## FUNDING

Grants-in-Aids from the Ministry of Education, Culture, Sports, Science and Technology of Japan; Ministry of Health, Labor and Welfare of Japan. Funding for open access charge: Innovative Cell Biology by Innovative Technology granted by the Japan Science and Technology Agency (JST).

*Conflict of interest statement*. None declared.

## REFERENCES

1. Black,D.L. (2003) Mechanisms of alternative pre-messenger RNA splicing. *Annu. Rev. Biochem.*, **72**, 291–336.
2. Jurica,M.S. and Moore,M.J. (2003) Pre-mRNA splicing: awash in a sea of proteins. *Mol. Cell*, **12**, 5–14.
3. Reed,R. (1996) Initial splice-site recognition and pairing during pre-mRNA splicing. *Curr. Opin. Gen. Dev.*, **6**, 215–220.
4. Parker,R., Siliciano,P.G. and Guthrie,C. (1987) Recognition of the TACTAAC box during mRNA splicing in yeast involves base pairing to the U2-like snRNA. *Cell*, **49**, 229–239.
5. Gao,K., Masuda,A., Matsuura,T. and Ohno,K. (2008) Human branch point consensus sequence is yUnAy. *Nucleic Acids Res.*, **36**, 2257–2267.
6. Zorio,D.A. and Blumenthal,T. (1999) Both subunits of U2AF recognize the 3′ splice site in Caenorhabditis elegans. *Nature*, **402**, 835–838.
7. Merendino,L., Guth,S., Bilbao,D., Martinez,C. and Valcarcel,J. (1999) Inhibition of msl-2 splicing by Sex-lethal reveals interaction between U2AF35 and the 3′ splice site AG. *Nature*, **402**, 838–841.
8. Kielkopf,C.L., Rodionova,N.A., Green,M.R. and Burley,S.K. (2001) A novel peptide recognition mode revealed by the X-ray structure of a core U2AF35/U2AF65 heterodimer. *Cell*, **106**, 595–605.
9. Mullen,M.P., Smith,C.W., Patton,J.G. and Nadal-Ginard,B. (1991) Alpha-tropomyosin mutually exclusive exon selection: competition between branchpoint/polypyrimidine tracts determines default exon choice. *Genes Dev.*, **5**, 642–655.
10. Coolidge,C.J., Seely,R.J. and Patton,J.G. (1997) Functional analysis of the polypyrimidine tract in pre-mRNA splicing. *Nucleic Acids Res.*, **25**, 888–896.

11. Soares,L.M., Zanier,K., Mackereth,C., Sattler,M. and Valcarcel,J. (2006) Intron removal requires proofreading of U2AF/3′ splice site recognition by DEK. *Science*, **312**, 1961–1965.
12. Wu,S., Romfo,C.M., Nilsen,T.W. and Green,M.R. (1999) Functional recognition of the 3′ splice site AG by the splicing factor U2AF35. *Nature*, **402**, 832–835.
13. Guth,S., Martinez,C., Gaur,R.K. and Valcarcel,J. (1999) Evidence for substrate-specific requirement of the splicing factor U2AF(35) and for its function after polypyrimidine tract recognition by U2AF(65). *Mol. Cell. Biol.*, **19**, 8263–8271.
14. Guth,S., Tange,T.O., Kellenberger,E. and Valcarcel,J. (2001) Dual function for U2AF(35) in AG-dependent pre-mRNA splicing. *Mol. Cell. Biol.*, **21**, 7673–7681.
15. Pacheco,T.R., Coelho,M.B., Desterro,J.M., Mollet,I. and Carmo-Fonseca,M. (2006) In vivo requirement of the small subunit of U2AF for recognition of a weak 3′ splice site. *Mol. Cell. Biol.*, **26**, 8183–8190.
16. Vorechovsky,I. (2006) Aberrant 3′ splice sites in human disease genes: mutation pattern, nucleotide structure and comparison of computational tools that predict their utilization. *Nucleic Acids Res.*, **34**, 4630–4641.
17. Lefevre,S.H., Chauveinc,L., Stoppa-Lyonnet,D., Michon,J., Lumbroso,L., Berthet,P., Frappaz,D., Dutrillaux,B., Chevillard,S. and Malfoy,B. (2002) A T to C mutation in the polypyrimidine tract of the exon 9 splicing site of the RB1 gene responsible for low penetrance hereditary retinoblastoma. *J. Med. Genet.*, **39**, E21.
18. Faustino,N.A. and Cooper,T.A. (2003) Pre-mRNA splicing and human disease. *Genes Dev.*, **17**, 419–437.
19. Wang,X.-H., Poh-Fitzpatrick,M., Chen,T., Malavade,K., Carriero,D. and Piomelli,S. (1995) Systematic screening for RNA with skipped exons - splicing mutations of the ferrochelatase gene. *Biochim. Biophys. Acta*, **1271**, 358–362.
20. Takahashi,I., Takahashi,T., Komatsu,M., Sato,T. and Takada,G. (2002) An exonic mutation of the GH-1 gene causing familial isolated growth hormone deficiency type II. *Clin. Genet.*, **61**, 222–225.
21. Okada,K., Inoue,A., Okada,M., Murata,Y., Kakuta,S., Jigami,T., Kubo,S., Shiraishi,H., Eguchi,K., Motomura,M. *et al.* (2006) The muscle protein Dok-7 is essential for neuromuscular synaptogenesis. *Science*, **312**, 1802–1805.
22. Ikeda,Y., Takagi,A., Nakata,Y., Sera,Y., Hyoudou,S., Hamamoto,K., Nishi,Y. and Yamamoto,A. (2001) Novel compound heterozygous mutations for lipoprotein lipase deficiency. A G-to-T transversion at the first position of exon 5 causing G154V missense mutation and a 5′ splice site mutation of intron 8. *J. Lipid Res.*, **42**, 1072–1081.
23. Petroulakis,E., Cao,Z., Clarke,J.T., Mahuran,D.J., Lee,G. and Triggs-Raine,B. (1998) W474C amino acid substitution affects early processing of the alpha-subunit of beta-hexosaminidase A and is associated with subacute G(M2) gangliosidosis. *Hum. Mutat.*, **11**, 432–442.
24. Kralovicova,J. and Vorechovsky,I. (2010) Allele-specific recognition of the 3′ splice site of INS intron 1. *Hum. Genet.*, **128**, 383–400.
25. Cartegni,L., Wang,J., Zhu,Z., Zhang,M.Q. and Krainer,A.R. (2003) ESEfinder: a web resource to identify exonic splicing enhancers. *Nucleic Acids Res.*, **31**, 3568–3571.
26. Smith,P.J., Zhang,C., Wang,J., Chew,S.L., Zhang,M.Q. and Krainer,A.R. (2006) An increased specificity score matrix for the prediction of SF2/ASF-specific exonic splicing enhancers. *Hum. Mol. Genet.*, **15**, 2490–2508.
27. Fairbrother,W.G., Yeh,R.F., Sharp,P.A. and Burge,C.B. (2002) Predictive identification of exonic splicing enhancers in human genes. *Science*, **297**, 1007–1013.
28. Wang,Z., Rolish,M.E., Yeo,G., Tung,V., Mawson,M. and Burge,C.B. (2004) Systematic identification and analysis of exonic splicing silencers. *Cell*, **119**, 831–845.
29. Zhang,X.H. and Chasin,L.A. (2004) Computational definition of sequence motifs governing constitutive exon splicing. *Genes Dev.*, **18**, 1241–1250.
30. Zhang,X.H., Kangsamaksin,T., Chao,M.S., Banerjee,J.K. and Chasin,L.A. (2005) Exon inclusion is dependent on predictable exonic splicing enhancers. *Mol. Cell. Biol.*, **25**, 7323–7332.
31. Goren,A., Ram,O., Amit,M., Keren,H., Lev-Maor,G., Vig,I., Pupko,T. and Ast,G. (2006) Comparative analysis identifies exonic splicing regulatory sequences–the complex definition of enhancers and silencers. *Mol. Cell*, **22**, 769–781.
32. Sahashi,K., Masuda,A., Matsuura,T., Shinmi,J., Zhang,Z., Takeshima,Y., Matsuo,M., Sobue,G. and Ohno,K. (2007) In vitro and in silico analysis reveals an efficient algorithm to predict the splicing consequences of mutations at the 5′ splice sites. *Nucleic Acids Res.*, **35**, 5995–6003.
33. Graveley,B.R. (2001) Alternative splicing: increasing diversity in the proteomic world. *Trends Genet.*, **17**, 100–107.
34. Kosaki,A., Nelson,J. and Webster,N.J. (1998) Identification of intron and exon sequences involved in alternative splicing of insulin receptor pre-mRNA. *J. Biol. Chem.*, **273**, 10331–10337.

Biochemical and Biophysical Research Communications 411 (2011) 143–149

Contents lists available at ScienceDirect

Biochemical and Biophysical Research Communications

journal homepage: www.elsevier.com/locate/ybbrc

# Molecular hydrogen inhibits lipopolysaccharide/interferon γ-induced nitric oxide production through modulation of signal transduction in macrophages

Tomohiro Itoh [a,b], Nanako Hamada [a], Riyako Terazawa [a], Mikako Ito [c], Kinji Ohno [c], Masatoshi Ichihara [d], Yoshinori Nozawa [a,e], Masafumi Ito [a,*]

[a] Department of Longevity and Aging Research, Gifu International Institute of Biotechnology, 1-1 Naka-fudogaoka, Kakamigahara, Gifu 504-0838, Japan
[b] Faculty of Agriculture, Kinki University, 3327-204 Nakamachi, Nara 631-8505, Japan
[c] Division of Neurogenetics, Center for Neurological Diseases and Cancer, Nagoya University Graduate School of Medicine, 65 Tsurumai, Showa-ku, Nagoya, Aichi 466-8550, Japan
[d] Department of Biomedical Sciences, College of Life and Health Sciences, Chubu University, 1200 Matsumoto-cho, Kasugai, Aichi 487-8501, Japan
[e] Department of Food and Health, Tokai Gakuin University, 5-68 Naka-kirinocho, Kakamigahara, Gifu 504-8511, Japan

ARTICLE INFO

*Article history:*
Received 7 June 2011
Available online 23 June 2011

*Keywords:*
Molecular hydrogen
Lipopolysaccharide/interferon γ
Macrophage
Signal transduction
Inflammatory arthritis

ABSTRACT

Molecular hydrogen has been reported to be effective for a variety of disorders and its effects have been ascribed to the reduction of oxidative stress. However, we have recently demonstrated that hydrogen inhibits type I allergy through modulating intracellular signal transduction. In the present study, we examined the hydrogen effects on lipopolysaccharide/interferon γ LPS/IFNγ-induced nitric oxide (NO) production in murine macrophage RAW264 cells. Treatment with hydrogen reduced LPS/IFNγ-induced NO release, which was associated with a diminished induction of inducible isoform of nitric oxide synthase (iNOS). Hydrogen treatment inhibited LPS/IFNγ-induced phosphorylation of apoptosis signal-regulating kinase 1 (ASK1) and its downstream signaling molecules, p38 MAP kinase and JNK, as well as IκBα, but did not affect activation of NADPH oxidase and production of reactive oxygen species (ROS). As ROS is an upstream activator of ASK1, inhibition of ASK1 by hydrogen without suppressing ROS implies that a potential target molecule of hydrogen should be located at the receptor or immediately downstream of it. These results suggested a role for molecular hydrogen as a signal modulator. Finally, oral intake of hydrogen-rich water alleviated anti-type II collagen antibody-induced arthritis in mice, a model for human rheumatoid arthritis. Taken together, our studies indicate that hydrogen inhibits LPS/IFNγ-induced NO production through modulation of signal transduction in macrophages and ameliorates inflammatory arthritis in mice, providing the molecular basis for hydrogen effects on inflammation and a functional interaction between two gaseous signaling molecules, NO and molecular hydrogen.



## 1. Introduction

Accumulating evidence suggest that molecular hydrogen is effective for a number of disorders including oxidative stress-related diseases and inflammatory diseases [1]. In animal disease models, inhalation of hydrogen gas protects against cerebral infarction [2], myocardial infarction, hepatic ischemia, neonatal hypoxic brain injury, small intestine and lung transplantation, zymosan-induced inflammation, inflammatory bowel disease and sepsis. Oral intake of hydrogen-rich water exerts beneficial effects on stress-induced learning impairment, atherosclerosis, Parkinson's disease, kidney transplantation and hearing disturbance. Infusion of hydrogen-rich saline also alleviates acute pancreatitis, spinal cord injury and obstructive jaundice. In humans, oral intake of hydrogen-rich water improves lipid and glucose metabolism in patients with diabetes and impaired glucose tolerance. In most of studies, hydrogen effects have been ascribed to the reduction of oxidative stress.

We have recently demonstrated a preventive effect of oral intake of hydrogen-rich water on type I allergy in a mouse model, which is not causally associated with oxidative stress [3]. In cultured mast cells, we investigated the underlying mechanisms and found that hydrogen attenuates degranulation by inhibiting the high affinity IgE receptor (FcεRI)-mediated signal transduction but not by reducing oxidative stress. Based on these observations, we proposed that modulation of signaling pathways may be an essential mechanism underlying hydrogen effects on a broad spectrum of diseases and that hydrogen may be a gaseous signaling molecule like nitric oxide (NO).

NO is involved in a variety of important physiological processes such as vasodilatation, neurotransmission and host defense against

* Corresponding author. Fax: +81 58 371 4412.
*E-mail address:* mito@giib.or.jp (M. Ito).

0006-291X/$ - see front matter © 2011 Elsevier Inc. All rights reserved.
doi:10.1016/j.bbrc.2011.06.116

invading pathogens [4]. However, an excessive amount of NO is detrimental, resulting in rheumatoid arthritis, gastritis, bowel inflammation and bronchitis [5,6]. In macrophages, NO is synthesized by inducible isoform of nitric oxide synthase (iNOS), which catalyzes the reaction of L-arginine to L-citrulline and NO, in response to various stimuli such as lipopolysaccharide (LPS), interferon (IFN), tumor necrosis factor α (TNFα) and interleukin 1β (IL1β) [7]. LPS binds to the cell surface receptor CD14, which triggers activation of toll like receptor 4 (TLR4) and the downstream signaling molecules such as IκB and mitogen-activated protein kinases (MAPKs) including c-Jun $NH_2$-terminal protein kinase (JNK), p38 MAP kinase and extracellular signal-regulated kinase (ERK) [8]. TLR4 signaling activates transcription factors such as nuclear factor kappa B (NFκB), activator protein 1 (AP1) and ELK1, culminating in the expression of pro-inflammatory genes including iNOS, cyclooxygenase 2 (COX2), TNFα and IFNβ. On the other hand, IFNβ and INFγ, respectively, bind to type I and type II IFN receptors expressed on the surface of macrophages, and activate Janus kinase (JAK)–signal transducers and activators of transcription (STAT) signaling, resulting in up-regulation of IFN regulatory factor 1 (IRF1) [9]. Both IRF1 and STAT1 bind to the iNOS promoter and enhance production of NO.

Previous reports have demonstrated that hydrogen treatment attenuates inflammation in animal models of inflammatory diseases such as zymosan-induced inflammation [10] and inflammatory bowel disease [11], but the underlying molecular mechanisms are not yet understood. According to our recent findings [3], we hypothesized that hydrogen might modulate the inflammatory signal transduction and that there might be a functional interaction between two gaseous signaling molecules, NO and molecular hydrogen. In the present study, we examined the effects of hydrogen on LPS/IFNγ-induced signal transduction and NO production in murine RAW264 macrophage cells. We also studied the hydrogen effects on anti-type II collagen antibody-induced arthritis in mice, a model for human rheumatoid arthritis.

## 2. Materials and methods

### 2.1. Antibodies

The antibodies to p-ASK1 (Ser967/Thr845), AKT, p-AKT, p44/42 MAP kinase (ERK1/2), p-p44/42 MAP kinase (Thr202/204), SAPK/JNK, p-SAPK/JNK (Thr180/Tyr204), p38 MAP kinase, p-p38 MAP kinase (Thr180/Tyr182), iNOS, COX2 TAK1, p-TAK1 (Ser412/Thr184/187), IκBα, p-IκBα (Ser32/36), NFκB p65, STAT1α and p-STAT1α (Tyr701) were purchased from Cell Signaling Technology (Beverly, CA, USA). The antibodies against $p22^{phox}$, $p47^{phox}$, $p67^{phox}$ and $gp91^{phox}$ were from Santa Cruz Biotechnology (Santa Cruz, CA, USA). Anti-ASK1, -histone H3 and -β-actin antibodies were obtained from Abcam (Cambridge, MA, USA), Upstate (Lake Placid, NY, USA) and Sigma–Aldrich (St. Louis, MO, USA), respectively.

### 2.2. Cell culture and hydrogen treatment

Murine macrophage RAW264 cells were purchased from RIKEN BioResource Center (Tsukuba, Japan) and cultured in Dulbecco's modified Eagle's medium (DMEM) containing 10% heat-inactivated fetal bovine serum (FBS), 100 U/ml of penicillin and 100 μg/ml streptomycin in a humidified atmosphere of 5% $CO_2$ at 37 °C. Hydrogen treatment was performed as described previously with a slight modification [3]. Briefly, cells seeded onto multi-well plates were incubated at 37 °C under a humidified condition of 75% $H_2$, 20% $O_2$ and 5% $CO_2$, or 95% air and 5% $CO_2$ in a small aluminum bag. After 24 h incubation in the presence of hydrogen, the hydrogen concentration in the culture media was about 0.3 ppm as measured by using the $H_2$-N hydrogen needle sensor (Unisense, Aarhus, Denmark). After treatment with or without hydrogen for 24 h, cells were treated with or without LPS (final concentration, 200 ng/ml) (Sigma–Aldrich) and IFNγ (final concentration, 25 ng/ml) (Millipore, Bedford, MA, USA), which was followed by incubation in the presence or absence of hydrogen.

### 2.3. Measurement of nitric oxide production

Cell culture media were centrifuged at 4 °C for 5 min and the supernatant was subjected to measurement of the amount of nitrite, a stable metabolite of NO, using the Griess reagent kit (Promega, Madison, WI, USA).

### 2.4. Western blot analysis

Whole cell extracts were prepared by lysing in RIPA buffer containing the complete protease inhibitor cocktail and the phosphatase inhibitor cocktail (Roche, Penzberg, Germany). The cytosolic and nuclear fractions were separated by the NE-PER nuclear and cytoplasmic extraction kit (Thermo Fisher Scientific, Waltham, MA, USA). The cytosolic and membrane fractions were isolated using the ProteoExtract subcellular proteome extraction kit (Merk KGaA, Darmstdt, Germany). Samples were subjected to sodium dodecyl sulfate–polyacrylamide gel electrophoresis (SDS–PAGE) and electroblotted onto PVDF membranes. Membranes were incubated with a primary antibody, followed by incubation with a horseradish peroxidase-conjugated secondary antibody. Immunolabeled proteins were detected using the ECL chemiluminescence kit (GE Healthcare, Piscataway, NJ, USA) and the LAS-4000 lumino-image analyzer (Fujifilm, Tokyo, Japan).

### 2.5. Quantitative RT-PCR

Total RNA was extracted from cells by the TRIzol reagent (Invitrogen, Carlsbad, CA, USA) followed by DNase I treatment. cDNA was synthesized using the PrimeScript reagent kit (Takara Bio, Ohtsu, Japan) and subjected to quantitative RT-PCR using the Thermal Cycler Dice real-time PCR system (TP800, Takara Bio). Primers for *iNOS* and *GAPDH* were purchased from Takara Bio. The expression level of *iNOS* gene was determined using the comparative $C_t$ method and normalized to that of *GAPDH*. The PCR consisted of 45 cycles (95 °C for 10 s, 60 °C for 40 s and 72 °C for 1 s) after an initial denaturation step (95 °C for 10 min).

### 2.6. Measurement of intracellular ROS levels

Intracellular levels of reactive oxygen species (ROS) were determined using a cell-permeable fluorescent probe, CM-$H_2$DCF-DA (Invitrogen). Cells were incubated with 10 μM CM-$H_2$DCF-DA for 1 h at 37 °C. After treatment, cells were washed twice with PBS and lysed in RIPA buffer. The absorbance of the lysates was measured with excitation at 490 nm and emission at 530 nm using the MTP-600 fluorometric imaging plate reader (Corona Electric, Ibaraki, Japan).

### 2.7. Hydrogen treatment of mice

Five-weeks-old female BALB/c Cr Slc mice (Japan SLC, Hamamatsu, Japan) were fed with either hydrogen-rich or control water *ad libitum*, as described previously [3]. Hydrogen-rich water packed in aluminum pouches was purchased from Blue Mercury (Tokyo, Japan). The hydrogen concentration of the hydrogen-rich water was approximately 1.0 ppm. The control water was prepared by gently stirring the hydrogen-rich water in open air for 24 h. This study was approved by the Animal Use Committee of the Gifu

International Institute of Biotechnology and the animals were maintained according to the guidelines for the care of laboratory animals of the Gifu International Institute of Biotechnology.

### 2.8. Anti-type II collagen antibody-induced arthritis in mice

Inflammatory arthritis was induced using the arthritogenic mouse monoclonal anti-type II collagen 5 clone antibody cocktail (Iwai Chemical, Tokyo, Japan). Seven-weeks-old mice, which were fed with either hydrogen-rich or control water for 2 weeks, were injected intravenously with 1 mg of the arthritogenic cocktail. Hydrogen treatment continued after the injection. Three days later, 25 μg of LPS (*Escherichia coli* O111:B4) was injected intraperitoneally. Two weeks after the antibody injection, we took photographs of the hind and front paws, evaluated the arthritis scores and measured the foot volume of hind paws using the plethysmometer (MK550M, Muromachi-kikai, Tokyo, Japan). The arthritis score was determined by grading each of four paws on a 0–4 scale [12]. Thus, the total arthritis score of a given mouse varies in the range 0–16.

### 2.9. Statistical analysis

All data were analyzed using Student's *t*-test or two-way ANOVA followed by Fisher's multiple range test.

## 3. Results

### 3.1. Hydrogen inhibits LPS/IFNγ-induced NO release from RAW264 macrophage cells

Hydrogen treatment for 24 h did not affect cell viability and proliferation (data not shown). In order to explore possible interaction between NO and hydrogen, we examined the effects of hydrogen on LPS/IFNγ-induced NO release from murine RAW264 macrophage cells. Treatment with hydrogen significantly reduced the NO levels in the culture media, the inhibitory effect being more pronounced at 12 h than at 6 h after LPS/IFNγ stimulation (Fig. 1A). These results suggest that there exists a functional relationship between NO and hydrogen.

### 3.2. Hydrogen inhibits LPS/IFNγ-induced iNOS expression

Stimulation with LPS/IFNγ up-regulates expression of pro-inflammatory genes such as iNOS and COX2. As shown in Fig. 1B, LPS/IFNγ stimulation resulted in a robust increase in protein expression of iNOS and COX2 at 6 h after treatment, which was markedly suppressed by treatment with hydrogen. Consistent with these findings, quantitative RT-PCR demonstrated that hydrogen inhibits LPS/IFNγ-induced mRNA expression of *iNOS* at 3 h after stimulation (Fig. 1C). These results indicate that hydrogen is capable of inhibiting LPS/IFNγ-induced expression of iNOS, which may account for suppression by hydrogen of LPS/IFNγ-induced NO release from macrophage cells (Fig. 1A).

### 3.3. Hydrogen inhibits LPS/IFNγ-mediated signal transduction

LPS signaling enhances phosphorylation of MAPKs and IκBα, and thereby activates transcription factors such as AP1, ELK1 and NFκB, whereas IFNγ signaling increases expression of IRF1 via activation of JAK–STAT signaling. These transcription factors activated or up-regulated by LPS/IFNγ stimulation bind to the iNOS promoter and enhance NO production. LPS/IFNγ stimulation enhanced phosphorylation of MAPKs including p38, JNK and ERK as well as AKT and STAT1α (Fig. 2A). Hydrogen treatment inhibited LPS/IFNγ-induced phosphorylation of p38 and JNK, but did not affect that of ERK, AKT and STAT1α.

Phosphorylation of IκB proteins leads to its degradation and NFκB translocation into the nucleus. As shown in Fig. 2B, LPS/IFNγ stimulation enhanced phosphorylation of IκBα and reduced its cytosolic level, which was associated with a decrease in NFκB p65 subunit in the cytosol and its increase in the nuclei. Treatment with hydrogen suppressed the LPS/IFNγ-induced activation of the NFκB pathway.

Taken together, these results suggest that hydrogen suppresses LPS/IFNγ-mediated signal transduction by inhibiting phosphorylation of p38, JNK and IκBα, resulting in reduced iNOS expression and NO production.

### 3.4. Hydrogen inhibits LPS/IFNγ-induced phosphorylation of ASK1

Among protein kinases activated by LPS/IFNγ, p38, JNK and IκBα were specifically inhibited by hydrogen (Fig. 2A and B). Apoptosis signal-regulating kinase 1 (ASK1), which is activated by endotoxins such as LPS, has been shown to activate both p38 and JNK MAPKs [13]. We thus investigated whether ASK1 phosphorylation is affected by hydrogen. As shown in Fig. 2C, phosphorylation of ASK1 at Ser967 and Thr845 caused by LPS/IFNγ stimulation was attenuated by hydrogen treatment. In contrast, LPS/IFNγ-induced phosphorylation of TGFβ-activated kinase 1 (TAK1) at Ser412 and Thr184/187, which, as well as ASK1, has been implicated in TNF receptor associated factor (TRAF)-dependent signaling pathways [14], was not affected by treatment with hydrogen. These results indicate that hydrogen inhibits LPS/IFNγ-induced phosphorylation of ASK1.

### 3.5. Hydrogen does not affect LPS/IFNγ-induced NOX activation and ROS production

It has been shown that ASK1 is activated by endotoxins such as LPS through ROS production, which in turn activates p38 and JNK MAPKs [15]. Furthermore, a direct link between ASK1 and NADPH oxidase (NOX) has been reported [16]. Here we investigated whether inhibition by hydrogen of LPS/IFNγ-induced ASK activation is mediated by suppression of NOX activation and ROS production. As shown in Fig. 3A, hydrogen treatment did not affect LPS/IFNγ-induced ROS production. For NOX activation, in response to LPS/IFNγ stimulation, the levels of the cytosolic subunits of NOX, $p47^{phox}$ and $p67^{phox}$, were decreased in the cytosolic fraction and increased in the membrane fraction (Fig. 3B). However, treatment with hydrogen did not influence the LPS/IFNγ-induced translocation of $p47^{phox}$ and $p67^{phox}$ to the membranes. These results suggest that hydrogen does not affect LPS/IFNγ-induced NOX activation and ROS production.

### 3.6. Oral intake of hydrogen-rich water ameliorates anti-type II collagen antibody-induced arthritis in mice

The findings that hydrogen suppressed LPS/IFNγ-induced NO production in cultured macrophage cells prompted us to examine whether oral intake of hydrogen-rich water could ameliorate anti-type II collagen antibody-induced arthritis in mice, a model for human rheumatoid arthritis [17]. In this mouse disease model, following the injection of anti-type II collagen-specific monoclonal antibody, LPS is injected to increase the incidence and severity of the disease. As shown in Fig. 4A, erythema and swelling of the hind and front paws were alleviated in mice treated with hydrogen-rich water compared with those treated with control water. The arthritis score was significantly lower in hydrogen-rich water-treated mice than in control water-treated mice (Fig. 4B). Both left and right hind paw volumes were decreased in hydrogen-treated mice

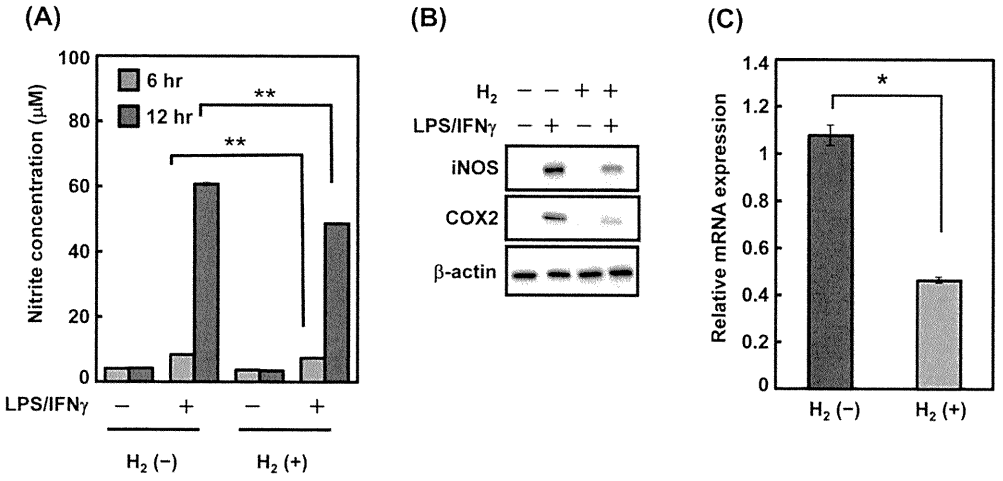


**Fig. 1.** Effects of hydrogen treatment on LPS/IFNγ-induced NO release and iNOS expression in RAW264 cells. RAW264 cells were incubated for 24 h in the presence or absence of hydrogen and then treated with or without LPS and IFNγ. (A) After incubation in the presence or absence of hydrogen for additional 6 and 12 h, cell culture media were harvested for measurement of nitrite, a stable metabolite of NO (mean ± SD, $n = 9$). Asterisks indicate statistical significance as determined by Student's $t$-test (**$p < 0.01$). (B) After incubation in the presence or absence of hydrogen for additional 6 h, cell lysates were harvested and subjected to Western blot analysis for iNOS, COX2 and β-actin. A representative blot from three independent experiments is shown. (C) After incubation in the presence or absence of hydrogen for additional 3 h, total RNA was harvested and subjected to quantitative RT-PCR for *iNOS* (mean ± SD, $n = 3$). Asterisks indicate statistical significance as determined by Student's $t$-test (*$p < 0.05$).

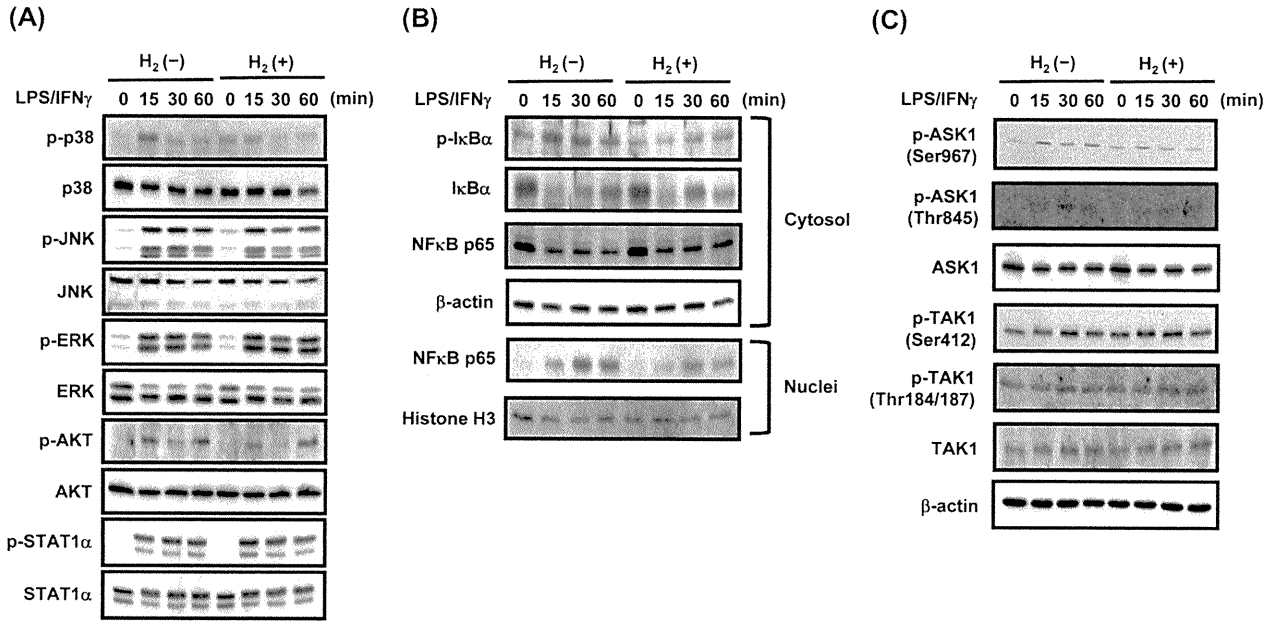


**Fig. 2.** Effects of hydrogen on LPS/IFNγ-mediated signal transduction in RAW264 macrophage cells. RAW264 macrophage cells were incubated for 24 h in the presence or absence of hydrogen and then treated with or without LPS and IFNγ. After incubation in the presence or absence of hydrogen for indicated time periods, cell lysates (A) and (C) and the cytosolic and nuclear fractions (B) were harvested and subjected to Western blot analysis for indicated proteins. A representative blot from three independent experiments is shown.

compared with control mice, but the statistical significance was observed only for the left hind paw ($p < 0.05$) (Fig. 4C). These results suggest that oral intake of hydrogen-rich water suppresses inflammation and alleviates arthritis in mice.

## 4. Discussion

Numerous papers have been published showing the efficacy of hydrogen treatment [1] since the first report in 2007 [2], in which specific scavenging of hydroxyl radical has been proposed as a mechanism accounting for the hydrogen effect. Most studies demonstrate reduced oxidative stress by hydrogen and assume that this is a major mechanism underlying the hydrogen effects. However, in type I allergy, hydrogen suppresses phosphorylation of FcεRI-associated Lyn and its downstream signaling molecules, which subsequently inhibits the NOX activity and reduces the generation of hydrogen peroxide [3]. Thus, we concluded that reduction of ROS by hydrogen in type I allergy is the consequence of inhibition of signal transduction, but not of direct radical scavenging activity.

Based on these findings, we hypothesized that hydrogen may ameliorate a wide variety of diseases, irrespective of their causal association with oxidative stress, through modulating yet

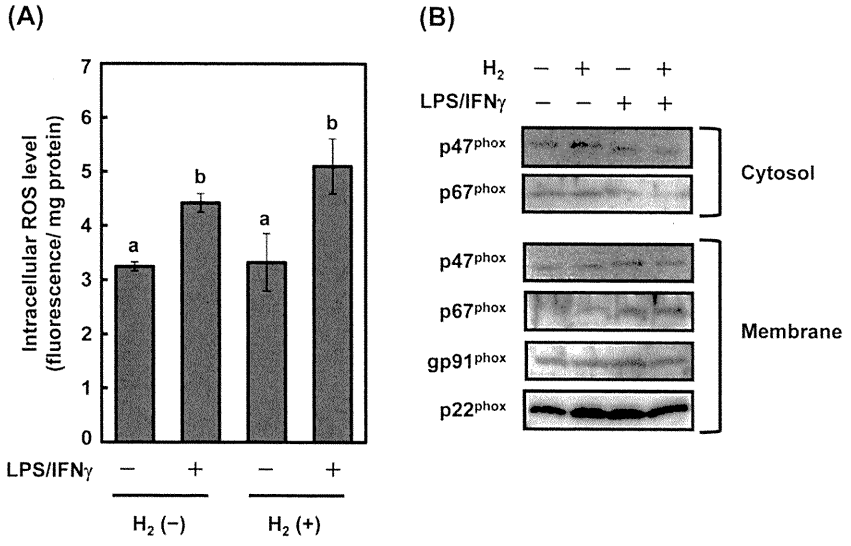


**Fig. 3.** Effects of hydrogen on LPS/IFNγ-induced NOX activation and ROS production in RAW264 macrophage cells. RAW264 macrophage cells were incubated for 24 h in the presence or absence of hydrogen. (A) Cells were incubated with 10 μM CM-$H_2$DCF-DA for 1 h in PBS and then treated with or without LPS/IFNγ. Three hours after incubation in the presence or absence of hydrogen, cell lysates were harvested and subjected to measurement of intracellular ROS (mean ± SD, $n = 6$). Statistical significance was determined by two-way ANOVA and Fisher's multiple range test ($p < 0.05$). (B) Cells were treated with or without LPS/IFNγ and then cultured in the presence or absence of hydrogen. Three hours later, the cytosolic and membrane fractions were separated and subjected to Western blot analysis for indicated proteins. A representative blot from three independent experiments is shown.

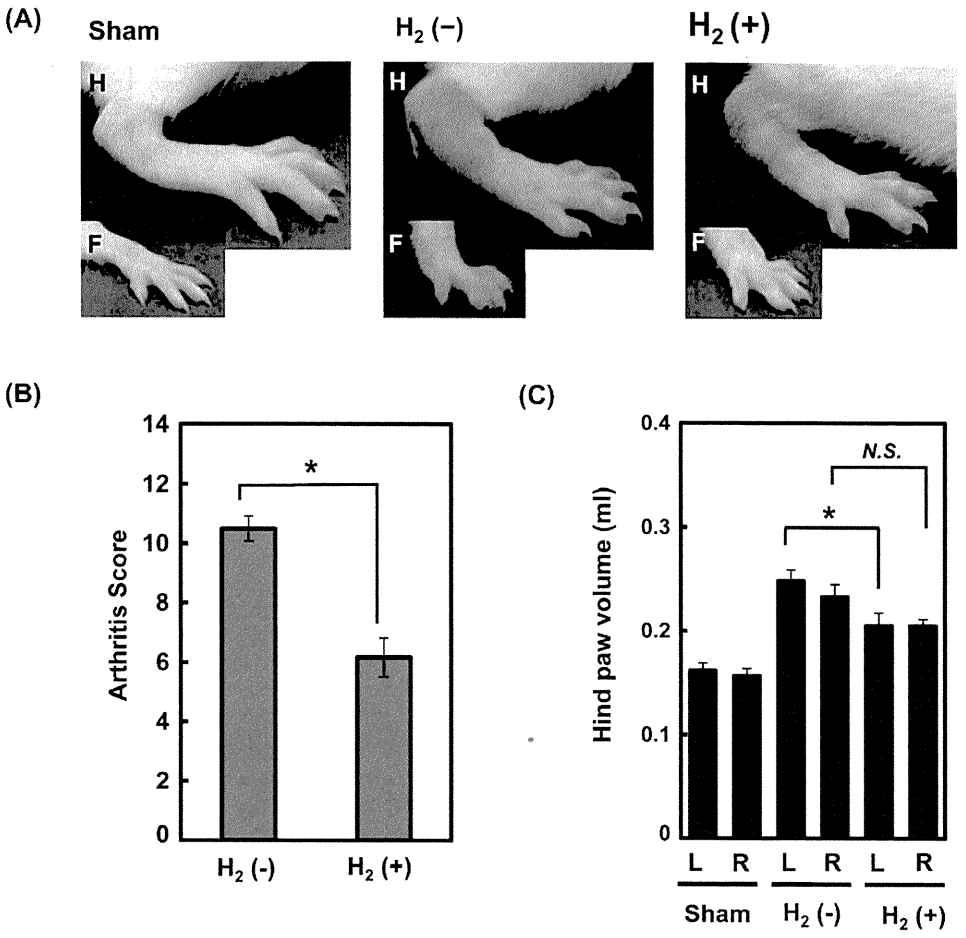


**Fig. 4.** Effects of oral intake of hydrogen-rich water on anti-type II collagen antibody-induced arthritis in mice. After treatment with or without hydrogen for 2 weeks, BALB/c Cr Slc female mice were injected intravenously with 1 mg of the arthritogenic mouse monoclonal anti-type II collagen antibody cocktail. Three days later, 25 μg of LPS was injected intraperitoneally. Two weeks after the antibody injection, photographs of the hind and front paws were taken (A), the arthritis score was evaluated (B), and the foot volume of hind paws was measured using the plethysmometer (C). Values are expressed as mean ± SD ($n = 5$). Asterisks indicate statistical significance as determined by Student's $t$-test (*$p < 0.05$). N.S., not statistically significant; L, left; R, right.